Profiling sensory neuron microenvironment after peripheral and central axon injury reveals key pathways for axon regeneration

Oshri Avraham[1], Rui Feng[1], Eric E. Ewan[1], Guoyan Zhao [1] and Valeria Cavalli[1,2,3 *]

[1] Department of Neuroscience, Washington University School of Medicine, St Louis 63110, Missouri, USA

[2] Center of Regenerative Medicine, Washington University School of Medicine, St. Louis, MO 63110, USA

[3] Hope Center for Neurological Disorders, Washington University School of Medicine, St. Louis, MO 63110, USA

Lead Contact:
Further information and requests for resources and reagents should be directed to and will be fulfilled by the Lead Contact Valeria Cavalli, cavalli@wustl.edu

***Correspondence to**: Valeria Cavalli, Department of Neuroscience, Washington University School of Medicine, Campus Box 8108, 4523 Clayton Ave, St. Louis, MO 63110-1093 Phone: 314 362 3540, Fax: 314 362 3446, E-mail: cavalli@wustl.edu

Abstract

Sensory neurons with cell bodies in dorsal root ganglia (DRG) represent a useful model to study axon regeneration. Whereas regeneration and functional recovery occurs after peripheral nerve injury, spinal cord injury or dorsal root injury is not followed by regenerative outcomes. This results in part from a failure of central injury to elicit a pro-regenerative response in sensory neurons. However, regeneration of sensory axons in peripheral nerves is not entirely cell autonomous. Whether the different regenerative capacities after peripheral or central injury result in part from a lack of response of macrophages, satellite glial cells (SGC) or other non-neuronal cells in the DRG microenvironment remains largely unknown. To answer this question, we performed a single cell transcriptional profiling of DRG in response to peripheral (sciatic nerve crush) and central injuries (dorsal root crush and spinal cord injury). Each cell type responded differently to peripheral and central injuries. Activation of the PPAR signaling pathway in SGC, which promotes axon regeneration after nerve injury, did not occur after central injuries. Treatment with the FDA-approved PPARα agonist fenofibrate, increased axon regeneration after dorsal root injury. This study provides a map of the distinct DRG microenvironment responses to peripheral and central injuries at the single cell level and highlights that manipulating non-neuronal cells could lead to avenues to promote functional recovery after CNS injuries.

Introduction:

Peripheral sensory neurons activate a pro-regenerative program after nerve injury to enable axon regeneration and functional recovery. In contrast, axons fail to regenerate after central nervous system injury, leading to permanent disabilities. Sensory neurons with cell bodies in dorsal root ganglia (DRG) represent one of the most useful models to study axon regeneration. Sensory neurons send a single axon which bifurcates within the ganglion; one axon proceeds centrally along the dorsal root into the spinal cord and the other proceeds along peripheral nerves. Whereas regeneration and functional recovery can occur after peripheral nerve injury, dorsal root injury or spinal cord injury is not followed by regenerative outcomes [1-5]. This results in part from a failure of central injury to elicit a pro-regenerative response in sensory neurons [5-9].

The dorsal root injury is a useful model to understand how to promote axon growth into the central nervous system [10]. Dorsal root disruption can occur in brachial plexus injuries, leading to paralysis of the affected arm [10]. Regeneration following dorsal root crush can occur along the growth-supportive environment of Schwann cells, but stops as the axons reach the transition between the peripheral nervous system and the central nervous system, termed the dorsal root entry zone, where a variety of inhibitory factors block further growth [10]. However dorsal root axonal growth occurs only at half the rate of peripheral axons [11, 12]. The histological difference between dorsal roots and peripheral nerve is not sufficient to alter the rate of axonal regeneration [11]. Rather, the availability of trophic factors and other target derived influences via the peripheral axon were suggested to prevent the upregulation of pro-regenerative genes such as *c-Jun* [2] or *Gap43* [13]. Interestingly, dorsal root injury causes up-regulation of the pro-regenerative gene *Atf3*[14], but only in large diameter neurons, whereas *Atf3* and *Jun* are upregulated in a majority of neurons after peripheral nerve injury [15-18]. Spinal cord injury also leads to activation of *Atf3* in large diameter neurons, but this is not sufficient to promote regenerative growth [19]. Another possibility explaining the slow growth capacity of axons in the injured dorsal root, is the contribution of non-neuronal cells.

Regeneration of axons in peripheral nerves is not cell autonomous. At the site of injury in the nerve, Schwann cells [20] and macrophages [21] contribute to promote axon regeneration. At the level of the DRG, macrophages are involved in eliciting a pro-regenerative response after peripheral but not central injury [21-24], with anti-inflammatory macrophages believed to be more involved in the regenerative process than pro-inflammatory macrophages [21]. How peripheral or central injury affects macrophage polarization remains unknown. We recently revealed that satellite glial cells (SGC), which completely surround sensory neuron soma, contribute to promote axon regeneration [25]. PPARα signaling downstream of fatty acid synthase in SGC promote axon regeneration in peripheral nerves, in part via regulating the expression of pro-regenerative genes in neurons, such as *Atf3* [25]. Whether the different regenerative capacities after peripheral or central injury result in part from a lack of response of macrophages, SGC or other non-neuronal cells in the DRG microenvironment remains largely unknown.

To unravel how neurons and non-neuronal cells in the DRG respond to central and peripheral injuries, we performed a comprehensive single cell transcriptional profiling of DRG cells after peripheral injury (sciatic nerve crush) and central injuries (dorsal root crush and spinal cord injury). Sciatic nerve crush injures approximately half the axons projecting into the peripheral nerves [26, 27] and dorsal root crush injures all axons projecting into the dorsal root. Dorsal column lesion of the spinal cord damages the ascending axon branches of most large diameter neurons and leaves the descending axon branches in the spinal cord intact [28 29, 30]. We found that gene expression changes occurred in neurons, endothelial cells, pericytes, Schwann cells, macrophages and SGC after peripheral nerve injury, but also occurred after dorsal root crush and spinal cord injury. However, each cell type responded differently to peripheral and central injuries. We show that SGC fail to activate the PPARα signaling pathway in response to dorsal root crush and downregulate this pathway in response to SCI. Using the PPARα agonist fenofibrate, an FDA-approved compound used to treat dyslipidemia [31], axon regeneration after dorsal root crush

was increased. These results indicate that the DRG microenvironment respond differently to central and peripheral axon injuries and that manipulating non-neuronal cells could lead to avenues to promote functional recovery after CNS injuries. Our data is available on a web-based resource for exploring changes in gene expression in DRG cells after central and peripheral injuries (https://mouse-drg-injury.cells.ucsc.edu/), which will aid the field to study the role of the DRG microenvironment in sensory function recovery after injury.

Results:

Profiling sensory neurons microenvironment following peripheral and central injuries

Neurons are the largest cells in the DRG but are outnumbered by other non-neuronal cells (Fig 1a). We quantified the proportion of neurons using a neuronal specific mouse line, *Baf53b-Cre* [32], to drive expression of GFP in the neuronal nuclei [33] (Fig.1b,c). FACS sorting analysis of dissociated DRG showed that GFP positive neurons represented only ~12.5% of all cells (Fig.1c). To assess the DRG microenvironment response to central or peripheral axon injury, we performed sciatic nerve crush (SNC) injury, dorsal root crush (DRC) injury or dorsal column spinal cord injury (SCI) (Fig 1d). SNC injures half the axons projecting into the sciatic nerve [26, 27] and is followed by activation of a pro-regenerative program that allows functional recovery [6, 34]. DRC injures all central axons projecting into the dorsal root and is followed by a slow regenerative growth that stops as axons reach the spinal cord [10 11, 12], providing an additional model to unravel the mechanisms promoting axon regeneration. SCI injures the ascending axons of a subset of large diameter neurons, leaving the descending axon branches in the spinal cord intact [28 29, 30], and is not followed by regenerative outcomes. We performed single cell RNA sequencing (scRNAseq) of L4,L5 mouse DRG in contralateral uninjured conditions (referred thereafter to naïve) and compared their transcriptional profile to DRG from mice 3 days after SNC, DRC and SCI using the Chromium Single Cell Gene Expression Solution (10X Genomics) (Fig.1e), as previously described [25]. An unbiased (Graph-based) clustering, using Partek flow analysis package,

identified 19 distinct cell clusters in the control and injured samples (Fig. S1a). The number of total sequenced cells from all conditions was 25,154 from 2 biological replicates for naïve, SCI and DRC conditions, and 1 biological replicate for SNC (Fig S1d), with an average of 45,000 reads per cell, 1,500 genes per cell and a total of 17,879 genes detected (see filtering criteria in the methods). To identify cluster-specific genes, we calculated the expression difference of each gene between that cluster and the average in the rest of the clusters (ANOVA fold change threshold >1.5). Examination of the cluster-specific marker genes revealed major cellular subtypes including neurons (Isl1), SGC (*Fabp7*), endothelial cells (*Pecam1*/CD31), Schwann cells (*Ncmap*), Pericytes (*KCNJ8*/Kir6.1), smooth muscle cells (PLN), macrophages (*Alf1*/Iba-1) and connective tissue (*Col1A1*) (Fig.1f,g and S1d and Supplementary Table 1). A t-SNE (t-distributed stochastic neighbor embedding) plot of all 25,154 cells combined from naïve and injury conditions revealed that the SGC and macrophages clusters contained the largest number of cells (Fig.1f,g). Comparison of population distribution between the different injury conditions revealed a reduction in the percentage of SGC after peripheral and central injuries, with an increase in the number of macrophages compared to naïve condition (Fig. 1g). Separate t-SNE plots for each condition uncovers major changes in cluster organization after SNC compared to naïve, with less variations after DRC and high similarity between naïve and SCI condition (Fig. 1h, S1b). We then determined the number of differentially expressed genes in six major cell types. Heat map of differential gene expression in the indicated cell types revealed that the magnitude of gene expression changes was the largest after SNC, but also occurred after DRC and SCI (Fig 1i), as previously suggested [19, 35]. We focused our analyses on neurons, endothelial cells, pericytes, Schwann cells, macrophages and SGC.

Neuronal response to peripheral and central injuries

Our scRNAseq protocol achieves recovery of non-neuronal cells with fewer neurons compared to other protocols that use single nuclear RNAseq [16, 25], thus limiting the depth of our

neuronal analysis. Nonetheless, we recovered a total of 257 neurons, 52 in naïve, 49 after SNC, 46 after DRC and 110 after SCI, which allowed us to examine their differential response to peripheral and central injuries. The majority of sensory neurons recovered were small diameter nociceptors (TrkA positive) with fewer LTMR's (TrkB positive) and proprioceptors (TrkC positive) [36] (Fig. 2a). Since the injured state induced by peripheral nerve injury is similar across neuronal subtypes [16 19], we pooled neuronal subtypes for each condition in our analyses and examined the differentially expressed genes in each injury condition (Supplementary Table2). There was little overlap in upregulated genes between the three injury conditions and more overlap in downregulated genes (Fig 2b). DRC elicited a robust transcriptional response with more DE genes upregulated compared to SNC, but fewer genes downregulated compared to SNC (Fig 2b). The larger number of DE genes after DRC compared to SNC (Fig 2b) could be due to the fact that SNC injures only half the axons projecting into the sciatic nerve [26, 27], whereas DRC injures all central axons projecting into the dorsal root. We thus examined expression of *Atf3* and *Sprr1a*, which represent markers of the injured state [16]. We found a similar number of neurons (20-30%) expressing *Sprr1a* and *Atf3 after* SNC *and* DRC (Fig. 2c,d,e). This might reflect the fact that we collected relatively few neurons with our approach and that these low numbers might not represent the true proportion of injured neurons in each condition. SCI, which directly injures large diameter neurons but not nociceptors [28], elicited a less robust transcriptional response compared to SNC (Fig. 2b). The number of DE genes we detected after SCI was similar to those observed in FACS-sorted nociceptors after compression SCI [37]. However, a small proportion of neurons (5%) which include both nociceptors (TrkA positive) and LTMRs (TrkB positive), expressed *Atf3* after SCI (Fig. 2d,e), consistent with prior findings [19]. KEGG pathway [38-40] analysis of DE genes in each condition identified distinct and shared pathways enriched after SNC, DRC and SCI injuries (Fig 2f). The p53 signaling pathway was enriched after both SNC and DRC, consistent with its role in neurite outgrowth and axon regeneration [41, 42]. Terpenoid backbone biosynthesis was enriched after all three injuries (Fig 2f). Terpenoid are intermediates in the biosynthesis of

cholesterol and studies using DRG cultures revealed that cholesterol is required for axonal growth [43-45], although more recent studies suggest that decreasing cholesterol levels promote axon growth [46, 47].

We next examined the expression of regeneration associated genes (RAGs), given their important roles in establishing a regenerative axon growth program [6, 48]. Heatmap of differential gene expression for selected RAGs revealed that SNC and DRC elicit a similar response, whereas the SCI response was restricted to the expression of *Atf3* and *Jun* (Fig 2g). We next examined ATF3 target genes, because ATF3 was shown to induce the transcriptional re-programming of all neuron subtypes after peripheral nerve injury [16]. We identified DE genes that have at least one ATF3 binding sites in the promoter region using Patser software [49] and ATF3 position weight matrix obtained from JASPAR database. We found a total of 721 ATF3 target genes regulated SNC, 792 in DRC and 283 by SCI. Genes that have ATF3 binding motifs are mainly unique to each condition (Fig 2h). KEGG pathway biological process analysis of ATF3 target genes further reveal the limited overlap between conditions (Fig S2a), and suggest that cAMP signaling pathway, which is required for axon regeneration [50], is regulated after DRC. We also found that *Atf3*, *Jun* and *Smad1*, which are believed to be exclusively neuronal, are highly expressed after SNC in multiple non-neuronal cell types (Fig S2b), whereas expression of *Sox11*, *Gap43* and *Sprr1a* after nerve injury was more specific to neurons (Fig. S2c). However, ATF3 expression at the protein level detected by immunofluorescence is specific to neurons [16, 25]. This analysis reveals that sensory neurons respond differently to SNC and DRC and that this difference may in part underlie the slower speed of regeneration after DRC compared to SNC. Other transcriptional program beyond classical RAGs or non-neuronal factor may also contribute to the low axon growth rate after DRC.

Alterations in blood-nerve-barrier markers in response to central and peripheral injuries

Blood-tissue barriers play an essential role in the maintenance and homeostasis of the tissue environment. Integrity of the peripheral nervous system is maintained by the blood-nerve-

barrier (BNB), which shares many structural features with the blood brain barrier [51]. An essential component of the BNB cellular architecture is tight junctions (TJ) in the endoneurial vascular endothelium or the perineurium that surrounds the nerve fascicle. Endothelial cells comprise the inner lining of vessels, while pericytes encompass blood microvessels such as blood capillaries [52]. Sensory ganglia are highly vascularized (Fig 3a) [53], with blood vessels in sensory ganglia being more permeable than their counterpart in the brain [54, 55] or the nerve[53, 56]. Unlike in the brain, pericytes do not fully cover the blood vessel in peripheral nerve [57]. We observed a similar situation in the DRG, with the presence of blood vessel not fully covered by pericytes (Fig 3b).

We examined changes in gene expression that occurred in endothelial cells and pericytes following peripheral and central injuries (Supplementary Table 3,4), as the magnitude of gene expression changes was the largest in these cells after SNC (Fig 1i). t-SNE plots of endothelial cells and pericytes demonstrated different clustering of cells in SNC or DRC, while similar clustering in naïve and SCI were observed (Fig. 3c,d). Increased BNB permeability in the nerve is linked to changes in the expression of TJ genes, in particular a reduced expression of ZO-1 (*Tjp1*) in endoneurial cells [51]. We thus examined the expression of tight junction (TJ) as well as adherens junction (AJ) genes. Heat map of TJ and AJ genes indicated that the response of barrier components was affected by SNC differently than DRC, with numerous junction genes being differentially expressed following SNC and DRC compared to naive and SCI condition (Fig. 3e,f). Changes in *Tjp1* and *Tjp2* expression suggest that the BNB is more permeable after SNC and DRC. KEGG pathway analysis of DE genes in endothelial cells and pericytes further suggest that the BNB may be differentially altered after SNC and DRC (Fig. 3g,h). The enrichment of the cell cycle pathway after SNC and DRC suggests that endothelial cell division may regulate blood vessel angiogenesis [58].

After nerve injury, dedifferentiation of Schwann cells into repair Schwann cells at the site of injury as well as resident macrophages in the nerve elicits breakdown of the BNB [59] [60] [51]. Although Schwann cells in the DRG are not in direct contact with injured axons, we found that

they undergo transcriptional changes that are distinct after peripheral and central injuries. t-SNE plots demonstrated different clustering of Schwann cells in SNC and DRC conditions, with similar clustering in naïve and SCI (Fig 3i). We next examined the expression of genes known to promote differentiation of Schwann cells into repair Schwann cells [61]. Heat map of such genes revealed non-overlapping changes after all three injuries (Fig. 3j). Notably, *Ngf,* which is known to promote myelination by Schwann cells in peripheral nerves [62] is downregulated after all injuries. VEGF is known to increase BNB permeability [63] and *Vegfb* is differentially regulated after peripheral and central injuries (Fig 3j), suggesting that Schwann cells may influence BNB permeability in the DRG. *Shh is* strongly upregulated after DRC. Shh signaling in Schwann cells in the DRG after SNC and DRC may have neuroprotective functions [64] and may facilitate axon regeneration [65]. KEGG analysis also revealed that the hedgehog signaling pathway and axon guidance is upregulated specifically after DRC (Fig. 3k). The hippo signaling pathway, which plays multiple cellular functions, such as proliferation, apoptosis, regeneration and organ size control [66] [67], is downregulated specifically after SCI and DRC. Key transcription factors in the Hippo pathway, *Yap* and *Bmp5* are downregulated after DRC and SCI, and upregulated after SNC (Supplementary Table 5). These results suggest that Schwann cell in the DRG respond differently to peripheral and central injuries, with central injury potentially limiting their plasticity.

Macrophages enhanced proliferation in response to peripheral but not central injuries

After nerve injury, breakdown of the BNB allows the influx of inflammatory cells at the site of injury in the nerve to promote repair [59] [60]. In addition to their role at the site of injury in the nerve, macrophages regulate axon regeneration and pain responses acting at the level of the ganglia [24] [23] [68]. Both resident and infiltrating macrophages were found in the DRG [21]. To understand if macrophages in the DRG include the two major macrophages subsets found in the nerve, snMac1 that reside in the endoneurium or snMac2 that reside in the connective tissue surrounding nerve fascicles [69], we analyzed the percent of DRG macrophages expressing marker genes for these

two subtypes. This analysis revealed that most DRG macrophages express the snMa1c genes (*Cbrr2, Mgl2*) (Fig. 4a, light blue), whereas few DRG macrophages express the snMac2 genes (*Retnnla, Clecl10a, Folr2)* (Fig. 4a, blue). The DRG macrophages, similarly to nerve macrophages [69 70], also express CNS associated microglia genes such as *Teme119*, *P2ry12* and *Trem2* (Fig. 4a, pink) and common microglia/macrophages markers *Ccl12*, ,*Gpr34*, *Gpr183*, *Hexb*, *Mef2c*, *St3gal6* and *Tagap* (Fig. 4a, green). The common macrophages markers *CD68*, *Emr1* and *Aif1*/Iba-1 were expressed in >80% of cells in the macrophage cluster (Fig. 4a, orange, Fig. S1d). These results suggest that DRG macrophages share similar properties to snMac1 residing in the nerve endoneurium and with CNS microglia.

We next examined the injury responses of DRG macrophages (Supplementary Table 6). t-SNE plot revealed different macrophage clustering in SNC and DRC, but a similar clustering in naïve and SCI (Fig. 4b). The number of macrophages increased after SNC compared to naïve and with lesser extent after DRC and SCI (Fig 1g). Macrophages displayed a similar gene expression profile in naive and SCI condition, but SNC and DRC elicited large changes in genes expression (Fig. 4c). KEGG pathway analysis revealed up regulation of cell cycle and DNA replication after SNC, while DRC and SCI macrophages mainly showed up regulation of metabolic pathways such as steroid biosynthesis and glycolysis/gluconeogenesis pathways (Fig. 4d). Interestingly, macrophages from all injury conditions down regulated genes related to antigen processing and presentation as well as genes involved in phagosome activity (Fig. 4d). Several studies suggested a predominant anti-inflammatory macrophage phenotype in the DRG following sciatic nerve injury [23, 24, 71, 72], but these studies were limited by immunofluorescence approaches. Heat map of cytokines and other macrophages polarization markers suggest that macrophages responses to injury in the DRG are complex and may not easily follow the classical pro-inflammatory and anti-inflammatory polarization scheme (Fig. 4e). Furthermore, expression of the anti-inflammatory marker gene *Arg1* was only detected after DRC and the pro-inflammatory marker *iNos* was not detected in any conditions. Hematopoietic cell lineage pathway, which is

involved in the formation of macrophages from myeloid cells, was down regulated specifically after DRC and SCI, but not after SNC (Fig. 4d). We next explored cell division in the macrophage cluster. The cell cycle and DNA replication pathways were upregulated only after SNC (Fig 4d). Heatmap analysis of the proliferation markers Ki67 (*MKI67*), *Cdk1* and *Top2a* further demonstrate higher expression of proliferation genes after SNC compared to naive macrophages and following central injuries (Fig. 4e). t-SNE plots overlaid with the proliferation marker genes *Mki67*, *Cdk1* and *Top2a* revealed expression mainly in a macrophage subtype following SNC (Fig. 4b,f). Immunostaining of DRG sections with the macrophage specific marker CD68 and the proliferation marker Ki67 revealed a higher number of CD68 and Ki67 positive cells after SNC and a trend towards an increase after DRC (Fig. 4g-i). Higher magnification in sections demonstrates co-expression of Ki67 in CD68 positive cells. Across all conditions, 80% of the Ki67 positive cells were also positive for CD68 (Fig 4j), which was also supported by the scRNAseq data, in which 83% of Ki67 expressing cells also expressed CD68, suggesting that macrophages represent a large proportion of proliferating cells in the DRG. This is consistent with the recent observation that macrophage expansion after nerve injury predominantly originate from resident macrophages proliferation [68]. These results highlight that central and peripheral nerve injury differently affect gene expression in macrophages and that a better understanding of these responses may highlight their role in pain and nerve regeneration.

A subset of macrophages expressing glial markers is increased by injury

The macrophage cluster was classified in our scRNAseq analysis by differential expression of macrophage specific markers such as *Cd68* and *Aif1*(Iba-1) (Fig. S1d, Table 1). However, a sub-cluster with 484 cells was classified as cluster 13 in an unbiased clustering (Fig. S1a). Examination of expression of top marker genes in macrophage (*CD68)* and SGC (*Fabp7*) revealed co-expression of both markers in cluster 13 (Fig. 5a, red circle). Macrophages (orange cells) and SGC (green cells) clusters were then specifically plotted for expression of *CD68* and

Fabp7, demonstrating that a subset of cells in these two clusters co-express macrophage and SGC markers (Fig. 5b). Violin plots of *CD68* and *Fabp7* expression across all cell types in the DRG further demonstrate that *CD68* and *Fabp7* are highly expressed in cluster 13, which we re-named 'immune glia' cluster (Fig. 5c). Dot plot analysis for expression of the macrophage marker genes *Aif1*, *Cd68*, *Cx3cr1* and *Emr1* and the glia marker genes *Fabp7*, *Mpz* and *Plp1*, support co-expression of both macrophage and satellite glial cell marker in the immune glia cluster (Fig. 5d). Co-staining of DRG sections with CD68 and Fabp7 further support co-expression of both markers in a small population of cells surrounding sensory neurons (Fig 5e upper, video 1,2). Macrophages can also be located in close proximity to SGC (Fig. 5e bottom), suggesting that their localization around sensory neurons can resemble SGC [73] [25]. To further characterize the immune glia cluster, DRG cells were re-clustered with the addition of the immune glia cluster (Fig 5f). Examination of the extent of the immune glia population in the DRG revealed that this is a rare population, representing ~1% of all DRG cells (Fig. 5g). Interestingly, the representation of immune glia in the DRG increased to ~ 2.5% after both peripheral and central injuries (Fig. 5g). t-SNE plot of immune glia cells revealed similar clustering across all conditions, suggesting similar gene expression that is not affected by injury (Fig. 5h). We then pooled the immune-glia cluster from all conditions and compared the DE genes (>1.5-fold change p-value<0.05 in immune glia (1,097 genes) to macrophages (2,469 genes) and SGC (2,331 genes). This analysis revealed a higher similarity of immune-glia cluster to macrophages (863 shared genes) than SGC (61 shared genes) (Fig. 5i, Supplementary Table 7). KEGG pathway analysis of immune glia and macrophage genes reveals similarity in immune-related pathways such as antigen processing and presentation, phagosome and hematopoietic cell lineage, while the top expressed pathways in SGC are completely different with enrichment of metabolic pathways (Fig. 5j). The 168 genes specifically expressed in immune glia revealed enrichment for pathways that are distinct from those shared with macrophages and SGC (Fig 5k). These results reveal the existence of a new cell population in DRG that shares feature of both immune and glial cells.

SGC do not represent a uniform cell population and at least four subtypes exist

We next determined if SGC represent a uniform glial population in the DRG or if subtypes exist in naïve conditions. We previously described that *Fabp7* is a specific marker gene for SGC in DRG and that the FABP7 protein is expressed in all SGC in the DRG (Fig. 6a) [25]. The DRG encompasses different types of sensory neurons such as nociceptors, mechanoreceptors and proprioceptors [16, 36], which each type controlling a different sensory function. To determine if SGC also exist as different subtypes in DRG, we examined the expression of other known SGC markers, *Cadh19*, *Kir4*.1(*kcnj10)* and GS*(Glul)* in addition to *Fabp7,* by pooling naïve SGC from our scRNAseq analysis. *Fabp7* labeled over 90% of SGC, whereas *Cadh19*, *Kir4.1* and *GS* labeled only ~50% of SGC (Fig 6b,c). An unbiased clustering of SGC from naïve DRG reveals 4 different subtypes with distribution between 15-30% for each subclusters that are represented by unique sets of gene expression (Fig. 6d, Supplementary Table 8). Overlay of *Pouf3f1*, *Gm13889*, *Aldh1l1* and *Scn7a* in t-SNE plots demonstrate cluster specific expression (Fig. 6e). KEGG pathway analysis of each sub-cluster highlights distinct functions, with cluster 1 enriched for glycan biosynthesis and MAPK signaling, cluster 2 enriched for cytokine and IL-17 signaling, cluster 3 enriched for steroid biosynthesis and terpenoid backbone biosynthesis and cluster 4 enriched for ECM and cell adhesion pathways (Fig. S3). To determine if a given subtypes is associated with a specific neuronal subtype, we examined expression of cluster 3 specific gene *Aldh1l1* using the *Aldh1l1-EGFP/Rpl10a* reporter mouse [74]. Aldh1l1 is typically used to label all astrocytes in the CNS and we found that *Aldh1l1* drove expression of *EGFP/Rpl10a* in a subset of SGC, consistent with the single cell data (Fig 6f). *EGFP/Rpl10a* expression was detected in SGC surrounding both TRKA positive neurons and TRKA negative neurons (Fig 6f), suggesting that cluster 3 SGC are not specifically associated to a given neuronal subtype. Our results are also consistent with the recent finding that *ALDH1L1-eGFP* mice express eGFP in a subset of SGC [75]. We next compared each SGC sub cluster with astrocytes [76], myelinating Schwann cells and non-myelinating Schwann cells [77]. Cluster 3, which expresses the astrocyte marker *Aldh1l1*

shares the most genes with astrocytes such as *Glul*, *kcnj10 (Kir4.1*) and *Glast* (*Slc1a3*) (Fig 6g,Supplementary Table 8). Cluster 4 shares more similarities with myelinated Schwann cells, consistent with the expression of *scn7a* in non-myelinating Schwann cells [78] (Fig 6h). Clusters 1 and 2 represent the most unique SGC subtypes (Fig 6g,h). Whether the SGC subtypes represent functionally distinct populations remains to be determined.

A distinct SGC cluster appears in response to peripheral nerve injury

We previously revealed the contribution of SGC to axon regeneration [25]. Specifically, we showed that PPARα signaling downstream of fatty acid synthase promotes axon regeneration after peripheral neve injury [25]. To determine if the different regenerative capacities after peripheral or central injury result in part from different responses in SGC, we examined the SGC responses to SCI and DRC compared to SNC. Separate clusters emerged in SGC after SNC and DRC injuries but were similar in naïve and SCI conditions (Fig 7a). We next determined if the 4 sub clusters identified in naïve conditions (Fig. 6d) are changing following the different injuries. An unbiased clustering of SGC in all conditions recognized 7 different sub clusters, in which cluster 1 to 4 represent the 4 clusters found in naïve conditions (Fig. 7b). The percentage of cells in clusters 2 and 5 remained largely unchanged after the different injuries, whereas the percentage of cells in cluster 1, 4, 6 and 7 were highly regulated by injury conditions (Fig. 7c). After SNC, cluster 1 (blue) decreased, whereas cluster 6 (light blue) emerged and accounted for 40% of all SGC. In contrast, SGC after SCI showed a decrease in cluster 4 (green), with cluster 7 appearing specifically after SCI (pink). Dot plot analysis further supports sub cluster changes in SGC following different injuries, revealing the percentage of cells in each cluster together with the level of expression of cluster specific genes (Fig. 7d). GFAP is a known marker of injured SGC [79, 80] and *GFAP* expression was observed in cluster 6 after SNC, but also in SGC after DRC in cluster 2, 3 and 4 (Fig. 7e,f). These results suggest that beyond *GFAP*, changes in SGC responses to SNC and DRC might explain the different axon regenerative capabilities in peripheral nerve and

dorsal root. We next performed KEGG pathway analysis of cluster 6 marker genes, which revealed enrichment for calcium signaling pathway and mineral absorption (Fig 7g). To further characterize the unique cluster 6 marker genes induced by SNC, we performed a transcription factor binding site analysis, which revealed enrichment for *Rest*, *PT53*, *Rad21*, *Ctcf* and *Zeb1* (Fig. 7h). We next used STRING to determine the functional protein interaction of these transcription factors and found that the transcription repressor CTCF was highly associated with the RAD21 and PT53*, less with* ZEB1 and not at all with REST (Fig. 7i). *Zeb1* is known to control epithelial-mesenchymal transition leading to a more plastic state [81], while *Rest* is involved in the signaling pathways regulating pluripotency [82], suggesting that cluster 6 adopts a more plastic state after SNC state that might play a role in nerve regeneration.

Activation of PPARα with fenofibrate increases axon regeneration after dorsal root crush

We recently revealed that satellite glial cells (SGC), which completely surround sensory neuron soma, contribute to promote axon regeneration following a peripheral injury [25]. To determine the overall biological differences in SGC responses to peripheral and central injuries we examined the up and down regulated biological processes and signaling pathways enriched in pooled SGC in each injury condition (Fig. 8a,b, Supplementary Table 9). Following nerve crush, SGC upregulate processes involving macrophage chemotaxis and migration, that might assist in the macrophage expansion in the DRG (Fig 8a). In contrast, after DRC, SGC upregulate genes involve in negative regulation of axon extension and guidance and negative regulation of chemotaxis (Fig 8a), that might explain, in part, the delayed axonal regeneration following DRC. After SCI, SGC upregulate genes involved in ECM assembly, myelination and chemical synaptic transmission. In agreement with our recent work [25], KEGG pathway analysis indicate that SGC upregulate fatty acid biosynthesis and PPARα signaling pathway after SNC (Fig 8b). However, none of these pathways were enriched after DRC and PPARα signaling was downregulated after

SCI (Fig 8b). We previously showed that the PPARα agonist fenofibrate, an FDA approved drug used to treat dyslipidemia [31] rescued the impaired axon growth in mice lacking fatty acid synthase in SGC [25]. However, there was no increased regeneration in control mice, suggesting that stimulating PPARα signaling following nerve injury does not stimulate further growth [25]. Since SGC do not activate PPARα after DRC (Fig 8b), a model in which axonal growth occurs at about half the rate of peripheral axons [11, 12], we tested if fenofibrate treatment improved axon regeneration after DRC. Mice were fed with fenofibrate or control diet for 2 weeks as described [25] and then underwent DRC injury. We measured the extent of axon regeneration past the injury site three days later by labeling dorsal root sections with SCG10, a marker for regenerating axons [83] (Fig. 8c). The crush site was determined according to highest SCG10 intensity along the nerve. First, we measured the length of the 10 longest axons, which reflect the extent of axon elongation, regardless of the number of axons that regenerate (Fig 8d). Second, we measured a regeneration index by normalizing the average SCG10 intensity at distances away from the crush site to the SCG10 intensity at the crush site (Fig. 8e). This measure takes into account both the length and the number of regenerating axons past the crush site. Both measurement methods revealed improved regeneration in mice treated with fenofibrate compared to control diet (Fig 8d,e). These results indicate that the lack of PPARα signaling in SGC after central injury contributes to the decreased regenerative ability. Whether PPARα activation could improve axon regeneration of dorsal column axons after SCI remains to be determined.

This study provides a map of the distinct DRG microenvironment responses to peripheral and central injuries at the single cell level and highlights that manipulating SGC in the DRG could lead to avenues to promote functional recovery after CNS injuries.

Discussion

Decades of research have focused on the signaling pathways elicited by injury in sensory neurons as central mechanisms regulating nerve repair. However, the microenvironment around sensory neurons is complex and composed of multiple cell types including satellite glial cells and immune cells. Transcriptional analysis of DRG cells in response to injury have been performed from bulk DRG tissue or from purified neurons. Therefore, the contribution of non-neuronal cells to the regenerative capacity of sensory neurons has remained poorly understood. Our unbiased single cell approach enables in depth characterization of the molecular profile of cells comprising the neuronal microenvironment in the DRG under peripheral and central acute injuries. Our analysis demonstrates major, yet distinct molecular changes in non-neuronal cells in response to peripheral nerve injury and dorsal root injury, with more limited responses after spinal cord injury. Our study provides a map of the distinct DRG microenvironment responses to peripheral and central injuries at the single cell level and highlights that manipulating non-neuronal cells could lead to avenues to promote functional recovery after spinal cord injury.

Our single cell approach does not allow recovery of many neurons and thus limits the depth of our neuronal analysis. However, our results support our previous studies showing that SCI and nerve injury elicits very distinct responses in sensory neurons [19]. Our results expand these findings and reveal that dorsal root crush leads to key RAG expression similar to nerve injury, suggesting that differential gene expression beyond RAGs and/or non-neuronal cells contribute to an axon generation speed that is half that of the peripheral nerve. Our observation that activating PPAR signaling in SGC increase the extend of axon regeneration after DRC support the contribution of non-neuronal cells. These results further highlight the importance of the DRG microenvironment in regenerative outcomes. In endothelial cells, pericytes, Schwann cells, macrophages and SGC, gene expression changes were the largest after peripheral injury, but also occurred after dorsal root crush and spinal cord injury. How non-neuronal cells sense a distant injury remains poorly understood. The mechanisms underlying SGC responses to nerve

injury have been proposed to depend on early spontaneous activity in injured neurons as well as retrograde signaling and direct bidirectional communication [79, 80]. Macrophages have been proposed to respond to chemokines expressed by injured neurons (such as CCL2) for their recruitment to the DRG after nerve injury [22, 23]. Our analysis of SGC suggest that they may also contribute to the increase in macrophage number in the DRG after nerve injury. Other cell types in the DRG have not been previously shown to respond to injury. How the cells sense injury and how they contribute to functional and physiological outcomes after peripheral or central injury remains to be determined.

The breakdown of the BNB in response to nerve damage can lead to neuronal dysfunction and contribute to the development of neuropathy [51]. While the impact of physical nerve damage or disease state such as diabetic neuropathy on the BNB are being studied [51], whether and how nerve injury affect the BNB in the sensory ganglion is not known. BNB leakage can give blood derived molecules direct access to sensory neurons and promote infiltration of inflammatory cells to engage inflammatory responses. Our results suggest that endothelial cells and pericytes respond differently to peripheral and central injuries, with alteration in expression of tight junction related genes, potentially underlying changes in BNB permeability. What would initiate these changes in endothelial cells remains unclear. Similarly to the situation in the nerve, Schwann cells and potentially macrophages may secrete factors such as VEGF and cytokines, altering endothelial cell function. Sympathetic innervation of blood vessels in the DRG following nerve injury, which depends in part on IL-6 signaling, may also underlie the changes observed in endothelial cells [84, 85].

In the injured nerve, Schwann cells guide regenerating axons to support distal innervation [20, 86]. To accomplish these regenerative functions, Schwann cells are reprogrammed to a repair state, which relies in part on the transition from an epithelial fate to a more plastic mesenchymal fate [87, 88]. Our studies highlight that away from the injury site in the DRG, Schwann cells also respond to injury in part by regulating the hippo pathway, a central pathway in cellular growth and

plasticity [66] [67]. The Hippo pathway is down regulated in Schwann cells after central but not peripheral injury. The transcription factor *Yap*, which is regulated by the hippo pathway, is upregulated after nerve injury but downregulated after both central injuries. The Nf2-Yap signaling was shown to play important roles in controlling the expansion of DRG progenitors and glia during DRG development [89]. These results suggest that Schwann cells in the DRG respond differently to distant peripheral and central injuries, and that central injury may limit their plasticity. What is the precise role of Schwann cell plasticity in the DRG remains to be determined. Interestingly, prior studies demonstrated that glial overexpression of NGF enhances neuropathic pain and adrenergic sprouting into DRG following chronic sciatic constriction in mice[90]. Since *Ngf* is downregulated in Schwann cell after all injuries, Schwann cells in the DRG may regulate pain and adrenergic sprouting after injury.

Macrophages are known to regulate regenerative responses. In the nerve, macrophages function primarily to assist Schwann cells for debris clearance. Nerve resident macrophages in naive conditions share features with CNS microglia [69, 70]. After nerve injury, resident macrophages represent only a small subset that secretes chemoattractants to recruit circulating monocytes-derived macrophages [69]. These recruited monocytes-derived macrophages express *Arg1* and represent the main macrophage population guiding nerve repair [69]. In the naïve DRG, we found that resident macrophages share similar properties with endoneurial macrophages in the nerve. However, *Arg1* expression is only observed after dorsal root crush and not after peripheral nerve injury or SCI. The increase in cell cycle marker after nerve injury suggest that the increase in macrophage numbers in the DRG comes from macrophage proliferation. The increase in IL-6, which has been associated with nerve regeneration [91, 92], is associated only with nerve injury and not central injuries. The differences in DRG macrophage transcriptional signatures after injury compared to nerve macrophages support the notion that they play very distinct roles. In the nerve macrophage assist Schwann cells for debris clearance, whereas in the DRG macrophages may have a local cellular signaling function. Our data also unravels the existence of a small proportion

of cells that share expression of macrophage and glial genes. These immune glia cells increase in number after all injuries. Previous studies suggested that injury to sensory neurons causes the attraction of macrophages into the ganglia, and that some macrophages even penetrate into the space between SGCs and neurons [93]. Our single cell profiling rather suggest that these cells represent a specific immune glia subtypes that share the spatial arrangement of SGC surrounding sensory neurons. These analyses suggest that immune cells in the DRG do not follow a strict classification and that complex subtypes exist in naive conditions that are further regulated by injury.

SGC have been previously characterized as a neural crest derived uniform glial population that plays a major role in pain [94]. Our single cell analysis reveals that SGC do not represent a uniform population but that several subtypes exist. In addition to the immune-glia discussed above, we identified four SGC clusters in naïve conditions and up to seven clusters after injury. The enrichment of different biological pathways in each cluster suggest that they each have a specialized function. Cluster 3 shares the most similarities with astrocytes and is enriched for PPARα signaling and fatty acid biosynthesis. Cluster 1 and 2 represent the most unique SGC subtypes. Interestingly, cluster 1 is enriched for calcium signaling pathway, which in SGC is known to play a role in pain [94]. Cluster 1 is also enriched for circadian rhythm. This is interesting because in astrocytes Fabp7 expression is circadian and implicates glial cells in the response or modulation of activity and/or circadian rhythms [95]. Fabp7 is expressed in all SGC but whether Fabp7 follows a circadian expression has not been determined. What will be important to determine in future studies is whether the most unique SGC subtypes (cluster 1 and 2) surround specific neuronal subtypes, or if a mosaic organization exists, with different SGC surrounding the same neuron.

The appearance of a specific cluster (cluster 6) after nerve injury suggest that this cluster plays an essential role in nerve injury responses. Pathway analysis of this cluster reveals enrichment for EMT genes. EMT is often linked to increased plasticity and stem cell activation

during tissue regeneration, suggesting that cluster 6 is related to plasticity of SGC. Cluster 6 is also enriched for the transcription factor REST, which in astrocyte regulates gliosecretion [96]. Whether cluster 6 represent an SGC 'reprogramming' to a new repair state awaits further investigation.

Our analysis of pooled SGC transcriptional response to nerve injury recently demonstrated that SGC activate PPARα signaling to promote axon regeneration in adult peripheral nerves [25]. Here we showed that this PPARα signaling pathway is not activated in SGC after central injures. Further, we demonstrate that the FDA approved PPARα agonist fenofibrate increased axon regeneration in the dorsal root, a model of poor sensory axon growth. Whether fenofibrate can improve regenerative outcomes in the spinal cord remains to be tested. It is encouraging to note that fenofibrate is used clinically to treat lipid disorders, and has unexpectedly been shown in clinical trials to have neuroprotective effects in diabetic retinopathy [97, 98] and in traumatic brain injury [99]. In rodent model, fenofibrate was shown to increase tissue sparing following spinal contusion injury in mice [100]. Together with the known role of SGC in pain and regeneration, the transcriptional profiling of SGC in response to peripheral and central injury highlights that manipulating non-neuronal cells could lead to avenues to promote functional recovery after CNS injuries as well as alleviate various pain syndromes.

Methods

Animals and Procedures

All surgical procedures were completed as approved by Washington University in St. Louis School of Medicine Institutional Animal Care and Use Committee's regulations. During surgery, 8-12-week-old female C57Bl/6 mice were anesthetized using 2% inhaled isoflurane. Sciatic nerve injuries were performed as previously described [80, 84] . Briefly, the sciatic nerve was exposed with a small skin incision (~1cm) and crushed for 5 seconds using #55 forceps. The wound was closed

using wound clips and injured L4 and L5 dorsal root ganglia were dissected at the indicated time post-surgery. Contralateral DRG served as uninjured control. For spinal cord injury (SCI), a small midline skin incision (~1cm) was made over the thoracic vertebrae at T9−T10, the paraspinal muscles freed, and the vertebral column stabilized with metal clamps placed under the T9/10 transverse processes. Dorsal laminectomy at T9/10 was performed with laminectomy forceps, the dura removed with fine forceps, and the dorsal column transversely cut using fine iridectomy scissors. Dorsal root injury was performed similarly as SCI, except that procedures were performed at the L2-L3 vertebral level, and fine forceps used to crush the right L4 dorsal root for 5 seconds. During dorsal root crush, the root is forcefully squeezed causing the disruption of nerve fibers without interrupting the endoneurial tube.

Mouse strains

8-12 weeks old male and female mice were used for all experiments, except for scRNAseq experiment, where only C57Bl/6 females were used. The *Sun1-sfGFP-myc* (INTACT mice: *R26-CAG-LSL-Sun1-sfGFP-myc*) [33], and *Baf53b-Cre* [32] was a generous gift from Dr. Harrison Gabel. The *Aldh1l1-EGFP/Rpl10a* transgenic line (B6;FVB-Tg(Aldh1l1-EGFP/Rpl10a)JD130Htz/J) [74] was a generous gift from Dr. Joseph Dougherty.

Single cell RNAseq

L4 and L5 DRG's from mice 8-12 weeks old were collected into cold Hank's balanced salt solution (HBSS) with 5% Hepes, then transferred to warm Papain solution and incubated for 20 min in 37ºC. DRG's were washed in HBSS and incubated with Collagenase for 20 min in 37ºC. Ganglia were then mechanically dissociated to a single cell suspension by triturating in culture medium (Neurobasal medium), with Glutamax, PenStrep and B-27. Cells were washed in HBSS+Hepes +0.1%BSA solution, passed through a 70-micron cell strainer. Hoechst dye was added to distinguish live cells from debris and cells were FACS sorted using MoFlo HTS with

Cyclone (Beckman Coulter, Indianapolis, IN). Sorted cells were washed in HBSS+Hepes+0.1%BSA solution and manually counted using a hemocytometer. Solution was adjusted to a concentration of 500cell/microliter and loaded on the 10X Chromium system. Single-cell RNA-Seq libraries were prepared using GemCode Single-Cell 3′ Gel Bead and Library Kit (10x Genomics). A digital expression matrix was obtained using 10X's CellRanger pipeline (Washington University Genome Technology Access Center). Quantification and statistical analysis were done with the Partek Flow package (Build version 9.0.20.0417).

Filtering criteria: Low quality cells and potential doublets were filtered out from analysis using the following parameters; total reads per cell: 600-15000, expressed genes per cell: 500-4000, mitochondrial reads <10%. A noise reduction was applied to remove low expressing genes <=1 count. Counts were normalized and presented in logarithmic scale in CPM (count per million) approach. An unbiased clustering (graph-based clustering) was done and presented as t-SNE (t-distributed stochastic neighbor embedding) plot, using a dimensional reduction algorithm that shows groups of similar cells as clusters on a scatter plot. Differential gene expression analysis performed using an ANOVA model; a gene is considered differentially-expressed (DE) if it has an p-value ≤ 0.05 and a fold-change ≥±2. The data was subsequently analyzed for enrichment of GO terms and the KEGG pathways using Partek flow pathway analysis. Partek was also used to generate figures for t-SNE and scatter plot representing gene expression.

ATF3 motif analysis

ATF3 position frequency matrix (MA0605.1) were obtained from JASPAR database (http://jaspar.genereg.net/). The Patser program calculates the probability of observing a sequence with a particular score or greater [49, 101] for the given matrix and determines the default cutoff score based on that P-value. Sequence 5kb upstream of ATG start codon of a given gene was scanned using Patser to identify ATF3 binding sites. Any gene with at least one ATF3 binding site was counted as ATF3 target gene. R package clusterProfiler [102] was used for GO and KEGG

pathway enrichment analysis and plotting. GO [103, 104] and KEGG pathway terms [38-40] with FDR corrected p-value < 0.05 were considered as significant.

Flow cytometry

Ganglia were enzymatically and mechanically dissociated to a single cell suspension as described above. Hoechst dye was added to distinguish live cells from debris. Cells were analyzed on a Attune NxT flow cytometer (ThermoFisher Scientific).

TEM

Mice were perfused with 2.5% glutaraldehyde with 4% paraformaldehyde in 0.1M Cacodylate buffer, followed by post fix. A secondary fix was done with 1% osmium tetroxide. For Transmission electron microscopy (TEM), tissue was dehydrated with ethanol and embedded with spurr's resin. Thin sections (70 nm) were mounted on mesh grids and stained with 8% uranyl acetate followed by Sato's lead stain. Sections were imaged on a Jeol (JEM-1400) electron microscope and acquired with an AMT V601 digital camera. (Washington University Center for Cellular Imaging).

Tissue Preparation and Immunohistochemistry

After isolation of either dorsal root or DRG, tissue was fixed using 4% paraformaldehyde for 1 hour at room temperature. Tissue was then washed in PBS and cryoprotected using 30% sucrose solution at 4C overnight. Next, the tissue was embedded in O.C.T., frozen, and mounted for cryosectioning. All frozen sections were cut to a width of 10µm for subsequent staining. For immunostaining of DRG and nerve sections, slides were washed 3x in PBS and then blocked in solution containing 10% goat serum in .2% Triton-PBS for 1 hour. Next, sections were incubated overnight in blocking solution containing primary antibody. The next day, sections were washed 3x with PBS and then incubated in a blocking solution containing a secondary antibody for 1 hour

at room temperature. Finally, sections were washed 3x with PBS and mounted using ProLong Gold antifade (Thermo Fisher Scientific). Images were acquired at 10x or 20x using a Nikon TE2000E inverted microscope and images were analyzed using Nikon Elements. Antibodies were as follow: SCG10/Stmn2 (1:1000; Novus catalog #NBP1-49461, RRID:AB_10011569), Tubb3/βIII tubulin antibody (BioLegend catalog #802001, RRID:AB_291637), Fabp7 (Thermo Fisher Scientific Cat# PA5-24949, RRID:AB_2542449), Ki67 (Abcam cat# ab15580), CD68 (Bio-Rad Cat# MCA1957 clone;FA-11), Islet-1 (Novus Biologicals, Cat# af1837-sp, 1:500) Stained sections with only secondary antibodies were used as controls. For Lectin injection, mice were deeply anesthetized by 1.5% isoflurane. 100ul of Lycopersicon esculentum (tomato) lectin (vector lab; Catalog#DL-1178-1) was used per mouse by injection into the tail vein. Mice were sacrificed after 20mins of injection. Samples were collected following the procedure described above. 20um thickness of DRG cryosections were used for immunofluorescence staining and image was captured under LSM880 confocal microscope.

Data collection and analyses. Data collection and analyses were performed blind to the conditions of the experiments. Single cell RNAseq analysis was performed in an unbiased manner using established algorithms.

Quantification and statistical analysis

Quantifications were performed by a blinded experimenter to injury type and treatment. Fiji (ImageJ) analysis software was used for immunohistochemistry images quantifications. Nikon Elements analysis software was used to trace regenerating axons in the dorsal root sections. Statistics was performed using GraphPad (Prism8) for t-test and one/two-way ANOVA followed by Bonferroni's multiple comparisons test. Error bars indicate the standard error of the mean (SEM).

Data availability

The raw Fastq files and the processed filtered count matrix for scRNA sequencing were deposited at the NCBI GEO database under the accession number GSE158892. Processed data are also available for visualization and download at https://mouse-drg-injury.cells.ucsc.edu/. Data analysis and processing was performed using commercial code from Partek Flow package at https://www.partek.com/partek-flow/

Acknowledgement

We would like to thank members of the Cavalli lab for valuable discussions. We thank Mayssa Mokalled for helpful discussion and comments on glial cells and spinal cord injury. We would like to thank Harrison Gabel for his generous gift of the *Baf53b*-cre mouse line and Joseph Dougherty for providing the *Aldh1l1-EGFP/Rpl10a* transgenic line. We gratefully acknowledge Greg Strout, Ross Kossina and Dr. James Fitzpatrick from the Washington University Center for Cellular Imaging (WUCCI), which is supported in part by Washington University School of Medicine, The Children's Discovery Institute of Washington University, and St. Louis Children's Hospital (CDI-CORE-2015-505 and CDI-CORE-2019-813) and the Foundation for Barnes-Jewish Hospital (3770) for assistance in acquiring and interpreting Transmission Electron Microscopy (TEM) data. We also thank Anushree Seth and Madison Mack in association with InPrint for illustration in Fig.1d. This work was funded in part by a post-doctoral fellowship from The McDonnell Center for Cellular and Molecular Neurobiology to O.A, by The McDonnell Center for Cellular and Molecular Neurobiology, NIH grant NS111719 and NS115492 to V.C.

Author contributions

O.A and V.C wrote the manuscript. O.A, E.E.E. and V.C designed research. O.A. performed single cell sequencing, bioinformatic analyses, *in vivo* experiments, analyzed the data and wrote the manuscript; R.F performed bioinformatic analyses, *in vivo* experiments, and analyzed the

data. E.E.E performed SCI surgical procedures and bioinformatic analyses. G.Z performed ATF3 target gene analysis. All authors edited and approved the manuscript.

Competing interests

The authors declare no competing interests.

Figure legends

Figure 1: DRG cells respond differently following peripheral and central injuries

(a) Representative TEM images of a DRG section showing neuronal cell bodies (pseudo-colored in purple) its enveloping SGC (pseudo-colored in turquoise) and other non-neuronal cells ((pseudo-colored in orange). n=4 biologically independent animals. Scale bar:20 µm

(b) *Baf53b-Cre* mice crossed with *Sun1GFP* show expression of GFP in all neuronal cell somas, co-labeled with the unique neuronal marker ISL1 (magenta). n=4 biologically independent animals, Scale bar: 50 µm

(c) Flow cytometry analysis of dissociated DRG cells from *Baf53b-Cre:Sun1GFP* mice. Scatter plot of fluorescence intensities of live Hoechst+ cells (x axis) and GFP+ (y axis). 12.5% of Hoechst+ cells are also GFP+ positive. n=3 biologically independent animals

(d) Diagram of mouse peripheral and central injury models

(e) Schematic of the experimental design for scRNAseq

(f) t-SNE plot of 25,154 cells from L4,L5 dissociated naïve and injured mouse DRG. 9 distinct cell clusters were assigned based on known marker genes.

(g) Fraction of each cell type within naive (6343 cells), SNC (4735 cells), DRC (7199 cells) and SCI (7063 cells) conditions. n=2 biologically independent experiments. Source data are provided as a Source Data file

(h) t-SNE plots of DRG cells separated by the different injury conditions, colored by cell type

(i) Heatmap of the number of differentially regulated genes in each cell type and injury condition (p-value<.05, Fold change>2)

Figure 2: Neuronal regeneration associated genes response to peripheral and central injuries

(a) Fraction of neuronal type within control and injury condition by expression of Trk receptors; TrkA (72%), TrkB (16%) and TrkC (12%). n=2 biologically independent experiments

(b) Venn diagrams for differentially up (left) and down (right) regulated genes after SNC, DRC or SCI. (p-value<.05, Fold change>2).

(c) t-SNE plot of DRG neurons colored by injury condition

(d) t-SNE plots of the regeneration associated genes *Atf3* and *Sprr1a* expression in DRG neurons after peripheral and central injury conditions

(e) Fraction of neurons expressing *Atf3* and *Sprr1a* in each injury condition

(f) Pathway analysis (KEGG 2019) of differentially upregulated (red) and downregulated (blue) genes in the Schwann cell cluster. n=2 biologically independent experiments. (p-value<.05, Fold change>2)

(g) Heatmap of log2 Fold change expression for selected RAGs after SNC, DRC and SCI compared to naïve

(h) UpSet plot of differentially expressed genes (DEGs). Bottom left: Graph of total number of DEGs (X axis) that were up- or down-regulated in each treatment condition (Y axis). Right: Intersection of sets of genes between different conditions. Each column corresponds to a set of genes whose expression were significantly changed in a condition (as indicated by the black dot of the first six columns) or sets of conditions (dots connected by lines below the X axis). The number of genes in each set appears above the column, while the conditions shared are indicated in the graphic below the column, with the conditions labeled on the left.

Figure 3: Molecular changes in non-neuronal cells in response to central and peripheral injuries

(a) Representative images of mouse DRG sections injected with Lycopersicon esculentum (Tomato) Lectin (magenta), labeling blood vessels and immunostained with FABP7 (green) labelling SGC. n=3 biologically independent animals. Scale bar: 50 µm.

(b) Representative TEM images of DRG sections focusing on blood vessels with the surrounding endothelial (pseudo-colored in purple) and pericytes (pseudo-colored in turquoise) n=4 biologically independent animals. Scale bar:2 µm

(c) t-SNE plot of DRG endothelial cells colored by injury condition

(d) t-SNE plot of DRG pericytes colored by injury condition

(e) Heatmap of Adherens junction (AJ) and Tight Junction (TJ) genes expression in endothelial cells by z-score for all injury conditions

(f) Heatmap of Adherens junction (AJ) and Tight Junction (TJ) genes expression in pericytes by z-score for all injury conditions

(g) Pathway analysis (KEGG 2019) of differentially upregulated (red) and downregulated (blue) genes in the endothelial cell cluster. n=2 biologically independent experiments. (p-value<.05, Fold change>2)

(h) Pathway analysis (KEGG 2019) of differentially upregulated (red) and downregulated (blue) genes in the pericyte cluster. n=2 biologically independent experiments. (p-value<.05, Fold change>2)

(i) t-SNE plot of DRG Schwann cells colored by injury condition

(j) Heatmap of fold change expression for selected repair Schwann cell genes after SNC, DRC and SCI compared to naïve

(k) Pathway analysis (KEGG 2019) of differentially upregulated (red) and downregulated (blue) genes in the Schwann cell cluster. n=2 biologically independent experiments. (p-value<.05, Fold change>2)

Figure 4: Macrophages undergo distinct transcriptional changes in response to central and peripheral injuries

(a) Fraction of uninjured cells expressing selected genes in the macrophage cluster. snMac2 (blue), snMac1 (light blue), specific microglia genes (pink), CNS microglia/macrophages (green) and common macrophage markers (yellow).

(b) t-SNE plot of mouse DRG macrophages colored by injury condition

(c) Heatmap of gene expression profile in macrophages by z-score for all injury conditions

(d) Pathway analysis (KEGG 2019) of differentially upregulated (red) and downregulated (blue) genes in the Macrophage cell cluster. n=2 biologically independent experiments. (p-value<.05, Fold change>2)

(e) Heatmap of M1, M2 macrophage markers, selected cytokines and proliferation marker gene expression by z- score for all injury conditions

(f) t-SNE overlay for expression of proliferation marker genes in pooled macrophage cluster from all injury conditions

(g) Representative images of immunofluorescence staining of DRG sections labelled with CD68 (green), Ki67 (white) and TUJ1 (red) from naïve mice, SNC, DRC and SCI injuries n=5 biologically independent animals. Scale bar: 50 μm.

(h) Quantification of area with CD68 expressing cells

(i) Quantification of Ki67 expressing cells normalized to DAPI

(j) Quantification of the percentage of cells expressing both Ki67 and CD68 out of all Ki67 positive cells. n=5 biologically independent animals. One-way analysis of variance (ANOVA)

followed by Bonferroni's multiple comparisons test. Data are presented as mean values ±SEM. Source data are provided as a Source Data file.

Figure 5: A subset of macrophages express glial markers and is increased by injury

(a) t-SNE of cells from all injury conditions overlay for expression of CD68 (red) and Fabp7 (green)

(b) plotting cells in the macrophage (orange) and SGC (green) clusters for expression of CD68 (y-axis) and Fabp7 (x-axis).

(c) Violin plots illustrate the expression signatures of CD68 and Fabp7 in distinct cell populations of naïve mouse DRG cells

(d) Dot plot of macrophage (black) and glial (blue) marker genes expression in the macrophage, SGC and immune-glia clusters. The percentage of cell expressing the gene is calculated as the number of cells in each cluster express the gene (>0 counts) divided by the total number of cells in the respective cluster. Expression in each cluster is calculated as mean expression of the gene relative to the highest mean expression of that gene across all clusters

(e) Representative images of immunofluorescence staining of DRG sections labelled with CD68 (green) and Fabp7 (magenta). Fluorescence intensity for CD68 and Fabp7 was measured around the neurons. n=3 biologically independent animals. Scale bar: 50 μm.

(f) t-SNE plot colored by classifications, separating immune glia (orange) from macrophage (green)

(g) Fraction of cells in the immune-glia cluster by injury condition. n=2 biologically independent experiments. Source data are provided as a Source Data file

(h) t-SNE plot of pooled immune-glia cells from all injury conditions

(i) Venn diagram of differentially expressed genes in the immune-glia cluster (1,097 genes) was compared to top differentially expressed genes in the macrophage cluster (2,469 genes) and the SGC (2331 genes).

(j) Pathway analysis (KEGG 2019) of differentially expressed genes in Macrophages, immune-glia and SGC

(k) Pathway analysis (KEGG 2019) of shared genes in immune-glia and Macrophage cluster (863 genes) Immune glia only (168 genes) and immune-glia and SGC (61 genes).

Figure 6: SGC represent a non-uniform cell population

(a) Representative images of immunofluorescence staining of DRG sections labelled with FABP7 (green) and TUJ1 (magenta). n=4 biologically independent animals. Scale bar: 100 µm, zoomed image: 50 µm

(b) t-SNE overlay for expression of SGC marker genes in pooled SGC cluster from naïve mice

(c) Fraction of cells in the SGC cluster expressing the SGC marker genes Fabp7, Cadh19, Kir4.1 and GS. (6<log gene counts).

(d) t-SNE plot of SGC cluster colored by subclusters (unbiased, Graph based clustering) with quantification of the fraction of cells in the different SGC subclusters out of total number of naïve SGC

(e) t-SNE overlay for expression of top differentially expressed genes in SGC subclusters

(f) Representative images of immunofluorescence staining of DRG sections from *Aldh1l1-EGFP/Rpl10a* mice (green) labelled with TUJ1 (magenta) and TRKA (cyan). n=4 biologically independent animals. Scale bar 50 µm

(g) Venn diagram comparing signature genes in SGC subclusters and astrocytes

(h) Venn diagrams comparing signature genes in SGC subclusters with myelinating (mySC) and non-myelinating (nmSC) Schwann cells markers

Figure 7: A distinct SGC cluster appears in response to peripheral nerve injury

(a) t-SNE plot of pooled SGC from naïve and injured mice, colored by injury condition

(b) t-SNE plot of pooled SGC from naïve and injured mice, colored by unbiased clustering

(c) Quantification of the fraction of cells for each subcluster in the different injury conditions

(d) Dot plot of SGC subclusters representation in the different injury conditions by z-score. The percentage of cells in a subcluster is divided by the total number of cells in the respective condition.

(e) t-SNE plots of pooled SGC colored by unbiased clustering, separated by injury condition

(f) t-SNE plots overlay for Gfap expression (blue), separated by injury condition

(g) Enriched signaling pathways (KEGG 2019) for top differentially expressed genes in subcluster 6

(h) Enriched TF (ENCODE and ChEA) in top differentially expressed genes in subcluster 6

(i) Protein-protein interaction of top TF expressed in subcluster 6 (String)

Figure 8: Axon regeneration is improved after dorsal root crush with fenofibrate treatment

(a) Enriched biological processes (GO 2018) for differentially up and down regulated genes in SGC after SNC, DRC and SCI

(b) Enriched signaling pathways (KEGG 2019) of differentially upregulated (red) and downregulated (blue) genes in the SGC cluster. n=2 biologically independent experiments. (p-value<.05, Fold change>2)

(c) Representative longitudinal sections of dorsal roots 3 days after injury from mice fed with fenofibrate or control diet, stained for SCG10. Arrows indicate the crush site, Scale Bar: 100 µm.

(d) Length of the longest 10 axons was measured in 10 sections for each nerve. Unpaired t-test. n=10 (control diet), n=8 (Fenofibrate diet) biologically independent animals. Data are presented as mean values ±SEM.

(e) Regeneration index was measured as SGC10 intensity normalized to the crush site. Two-way ANOVA followed by Bonferroni's multiple comparisons test. n=10 (control diet), n=8 (Fenofibrate diet) biologically independent animals. Data are presented as mean values ±SEM.

Supplementary Figures

Supplementary Figure 1: scRNAseq analysis of naïve and injured mouse DRG, related to Figure 1

(a) t-SNE plot of naïve and injured mouse DRG cells where 19 distinct cell clusters were identified by unbiased, Graph based clustering

(b) t-SNE plot of naïve and injured mouse DRG cells colored by injury condition

(c) t-SNE plot of naïve and injured mouse DRG cells colored by batch

(d) t-SNE overlay for expression of marker genes for different cell populations including Pecam/CD31 for endothelial cells, Col1a1 for connective tissue, Ncmap for Schwann cells, Isl1 for neurons, Kcnj8 for pericytes, Pln for smooth muscle cells, Fabp7 for SGC and Aif1/Iba-1 for Macrophages. The relative levels of expression are presented as a red color gradient on the left.

Supplementary Figure 2: Enriched pathways and RAG expression in neurons after injury, related to Figure 2

(a). GO enrichment analysis of ATF3 target genes in the indicated condition showing enriched terms in the Biological Processes (BP) category.

(b) Violin plots illustrate the expression signatures of the RAGs Atf3, Jun and Smad1 in distinct cell populations of DRG cells after SNC

(c) Violin plots illustrate the expression signatures of the RAGs Sox11, Gap43 and Sprr1a in distinct cell populations of DRG cells after SNC

Supplementary Figure 3: Unique enriched pathways of SGC subclusters, related to Figure 6

Enriched signaling pathways (KEGG 2019) for top differentially expressed genes in each SGC subcluster

Supplementary Tables

Supplementary Table 1
Top 10 differentially expressed genes per cluster relative to all other clusters.

Supplementary Table 2
Differentially regulated genes in the neuron cluster after SNC, DRC or SCI. (p-value<.05, Fold change>2).

Supplementary Table 3
Differentially regulated genes in the endothelial cluster after SNC, DRC or SCI. (p-value<.05, Fold change>2).

Supplementary Table 4
Differentially regulated genes in the pericyte cluster after SNC, DRC or SCI. (p-value<.05, Fold change>2).

Supplementary Table 5
Differentially regulated genes in the Schwann cell cluster after SNC, DRC or SCI. (p-value<.05, Fold change>2).

Supplementary Table 6
Differentially regulated genes in the macrophage cluster after SNC, DRC or SCI. (p-value<.05, Fold change>2).

Supplementary Table 7
Differentially expressed genes in the immune-glia cluster, macrophage cluster and SGC cluster relative to all other clusters.

Supplementary Table 8
Differentially expressed genes in SGC subclusters and their overlap with differentially expressed genes in Astrocytes, nmSC and mySC

Supplementary Table 9
Differentially regulated genes in the SGC cluster after SNC, DRC or SCI. (p-value<.05, Fold change>2).

Supplementary Video 1
3D video of image shown in Figure 5e

References

1. Schwaiger, F.W.*, et al.* Peripheral but not central axotomy induces changes in Janus kinases (JAK) and signal transducers and activators of transcription (STAT). *Eur J Neurosci* **12**, 1165-1176 (2000).
2. Broude, E., McAtee, M., Kelley, M.S. & Bregman, B.S. c-Jun expression in adult rat dorsal root ganglion neurons: differential response after central or peripheral axotomy. *Experimental neurology* **148**, 367-377 (1997).
3. Weng, Y.L.*, et al.* An Intrinsic Epigenetic Barrier for Functional Axon Regeneration. *Neuron* **94**, 337-346 e336 (2017).
4. Cho, Y.*, et al.* Activating Injury-Responsive Genes with Hypoxia Enhances Axon Regeneration through Neuronal HIF-1alpha. *Neuron* **88**, 720-734 (2015).
5. Loh, Y.E.*, et al.* Comprehensive mapping of 5-hydroxymethylcytosine epigenetic dynamics in axon regeneration. *Epigenetics* **12**, 77-92 (2017).
6. Mahar, M. & Cavalli, V. Intrinsic mechanisms of neuronal axon regeneration. *Nat Rev Neurosci* **19**, 323-337 (2018).
7. Puttagunta, R.*, et al.* PCAF-dependent epigenetic changes promote axonal regeneration in the central nervous system. *Nat Commun* **5**, 3527 (2014).
8. Kadoya, K.*, et al.* Combined intrinsic and extrinsic neuronal mechanisms facilitate bridging axonal regeneration one year after spinal cord injury. *Neuron* **64**, 165-172 (2009).
9. Palmisano, I.*, et al.* Epigenomic signatures underpin the axonal regenerative ability of dorsal root ganglia sensory neurons. *Nat Neurosci* (2019).
10. Smith, G.M., Falone, A.E. & Frank, E. Sensory axon regeneration: rebuilding functional connections in the spinal cord. *Trends Neurosci* **35**, 156-163 (2012).
11. Wujek, J.R. & Lasek, R.J. Correlation of axonal regeneration and slow component B in two branches of a single axon. *The Journal of neuroscience : the official journal of the Society for Neuroscience* **3**, 243-251 (1983).
12. Oblinger, M.M. & Lasek, R.J. A conditioning lesion of the peripheral axons of dorsal root ganglion cells accelerates regeneration of only their peripheral axons. *The Journal of neuroscience : the official journal of the Society for Neuroscience* **4**, 1736-1744 (1984).
13. Schreyer, D.J. & Skene, J.H. Injury-associated induction of GAP-43 expression displays axon branch specificity in rat dorsal root ganglion neurons. *J Neurobiol* **24**, 959-970 (1993).
14. Huang, W.L.*, et al.* Spinal cord compression and dorsal root injury cause up-regulation of activating transcription factor-3 in large-diameter dorsal root ganglion neurons. *The European journal of neuroscience* **23**, 273-278 (2006).
15. Tsujino, H.*, et al.* Activating transcription factor 3 (ATF3) induction by axotomy in sensory and motoneurons: A novel neuronal marker of nerve injury. *Mol Cell Neurosci* **15**, 170-182 (2000).
16. Renthal, W.*, et al.* Transcriptional Reprogramming of Distinct Peripheral Sensory Neuron Subtypes after Axonal Injury. *Neuron* (2020).
17. Seijffers, R., Mills, C.D. & Woolf, C.J. ATF3 increases the intrinsic growth state of DRG neurons to enhance peripheral nerve regeneration. *The Journal of neuroscience : the official journal of the Society for Neuroscience* **27**, 7911-7920 (2007).

18. Chandran, V.*, et al.* A Systems-Level Analysis of the Peripheral Nerve Intrinsic Axonal Growth Program. *Neuron* **89**, 956-970 (2016).
19. Ewan, E.E., Carlin, D., Goncalves, T.M., Zhao, G. & Cavalli, V. Ascending dorsal column sensory neurons respond to spinal cord injury and downregulate genes related to lipid metabolism. *bioRxiv* **https://doi.org/10.1101/2020.05.07.083584** (2020).
20. Jessen, K.R. & Mirsky, R. The repair Schwann cell and its function in regenerating nerves. *J Physiol* **594**, 3521-3531 (2016).
21. Zigmond, R.E. & Echevarria, F.D. Macrophage biology in the peripheral nervous system after injury. *Prog Neurobiol* **173**, 102-121 (2019).
22. Niemi, J.P., DeFrancesco-Lisowitz, A., Cregg, J.M., Howarth, M. & Zigmond, R.E. Overexpression of the monocyte chemokine CCL2 in dorsal root ganglion neurons causes a conditioning-like increase in neurite outgrowth and does so via a STAT3 dependent mechanism. *Experimental neurology* **275 Pt 1**, 25-37 (2016).
23. Niemi, J.P.*, et al.* A critical role for macrophages near axotomized neuronal cell bodies in stimulating nerve regeneration. *The Journal of neuroscience : the official journal of the Society for Neuroscience* **33**, 16236-16248 (2013).
24. Kwon, M.J.*, et al.* Contribution of macrophages to enhanced regenerative capacity of dorsal root ganglia sensory neurons by conditioning injury. *The Journal of neuroscience : the official journal of the Society for Neuroscience* **33**, 15095-15108 (2013).
25. Avraham, O.*, et al.* Satellite glial cells promote regenerative growth in sensory neurons. *Nature Communications* **volume 11, Article number: 4891 (2020)** (2020).
26. Laedermann, C.J., Pertin, M., Suter, M.R. & Decosterd, I. Voltage-gated sodium channel expression in mouse DRG after SNI leads to re-evaluation of projections of injured fibers. *Molecular pain* **10**, 19 (2014).
27. Rigaud, M.*, et al.* Species and strain differences in rodent sciatic nerve anatomy: implications for studies of neuropathic pain. *Pain* **136**, 188-201 (2008).
28. Niu, J.*, et al.* Modality-based organization of ascending somatosensory axons in the direct dorsal column pathway. *The Journal of neuroscience : the official journal of the Society for Neuroscience* **33**, 17691-17709 (2013).
29. Zheng, B., Lorenzana, A.O. & Ma, L. Understanding the axonal response to injury by in vivo imaging in the mouse spinal cord: A tale of two branches. *Experimental neurology* **318**, 277-285 (2019).
30. Attwell, C.L., van Zwieten, M., Verhaagen, J. & Mason, M.R.J. The Dorsal Column Lesion Model of Spinal Cord Injury and Its Use in Deciphering the Neuron-Intrinsic Injury Response. *Dev Neurobiol* **78**, 926-951 (2018).
31. Rosenson, R.S. Fenofibrate: treatment of hyperlipidemia and beyond. *Expert Rev Cardiovasc Ther* **6**, 1319-1330 (2008).
32. Zhan, X.*, et al.* Generation of BAF53b-Cre transgenic mice with pan-neuronal Cre activities. *Genesis* **53**, 440-448 (2015).
33. Mo, A.*, et al.* Epigenomic Signatures of Neuronal Diversity in the Mammalian Brain. *Neuron* **86**, 1369-1384 (2015).
34. He, Z. & Jin, Y. Intrinsic Control of Axon Regeneration. *Neuron* **90**, 437-451 (2016).

35. Stam, F.J.*, et al.* Identification of candidate transcriptional modulators involved in successful regeneration after nerve injury. *The European journal of neuroscience* **25**, 3629-3637 (2007).
36. Usoskin, D.*, et al.* Unbiased classification of sensory neuron types by large-scale single-cell RNA sequencing. *Nature neuroscience* **18**, 145-153 (2015).
37. Yasko, J.R., Moss, I.L. & Mains, R.E. Transcriptional Profiling of Non-injured Nociceptors After Spinal Cord Injury Reveals Diverse Molecular Changes. *Front Mol Neurosci* **12**, 284 (2019).
38. Kanehisa, M. & Goto, S. KEGG: kyoto encyclopedia of genes and genomes. *Nucleic acids research* **28**, 27-30 (2000).
39. Kanehisa, M., Sato, Y., Furumichi, M., Morishima, K. & Tanabe, M. New approach for understanding genome variations in KEGG. *Nucleic acids research* **47**, D590-D595 (2019).
40. Kanehisa, M. Toward understanding the origin and evolution of cellular organisms. *Protein Sci* **28**, 1947-1951 (2019).
41. Di Giovanni, S.*, et al.* The tumor suppressor protein p53 is required for neurite outgrowth and axon regeneration. *EMBO J* **25**, 4084-4096 (2006).
42. Ma, J.J.*, et al.* Telomerase Reverse Transcriptase and p53 Regulate Mammalian Peripheral Nervous System and CNS Axon Regeneration Downstream of c-Myc. *The Journal of neuroscience : the official journal of the Society for Neuroscience* **39**, 9107-9118 (2019).
43. Posse de Chaves, E., Vance, D.E., Campenot, R.B. & Vance, J.E. Axonal synthesis of phosphatidylcholine is required for normal axonal growth in rat sympathetic neurons. *The Journal of cell biology* **128**, 913-918 (1995).
44. Vance, J.E., Campenot, R.B. & Vance, D.E. The synthesis and transport of lipids for axonal growth and nerve regeneration. *Biochim Biophys Acta* **1486**, 84-96 (2000).
45. Vance, J.E., Pan, D., Campenot, R.B., Bussiere, M. & Vance, D.E. Evidence that the major membrane lipids, except cholesterol, are made in axons of cultured rat sympathetic neurons. *J Neurochem* **62**, 329-337 (1994).
46. Lee, J.*, et al.* The stem cell marker Prom1 promotes axon regeneration by down-regulating cholesterol synthesis via Smad signaling. *Proceedings of the National Academy of Sciences of the United States of America* **117**, 15955-15966 (2020).
47. Rosello-Busquets, C.*, et al.* Cholesterol Depletion Regulates Axonal Growth and Enhances Central and Peripheral Nerve Regeneration. *Front Cell Neurosci* **13**, 40 (2019).
48. Fagoe, N.D., van Heest, J. & Verhaagen, J. Spinal cord injury and the neuron-intrinsic regeneration-associated gene program. *Neuromolecular medicine* **16**, 799-813 (2014).
49. Hertz, G.Z. & Stormo, G.D. Identifying DNA and protein patterns with statistically significant alignments of multiple sequences. *Bioinformatics* **15**, 563-577 (1999).
50. Spencer, T. & Filbin, M.T. A role for cAMP in regeneration of the adult mammalian CNS. *J Anat* **204**, 49-55 (2004).
51. Richner, M.*, et al.* Functional and Structural Changes of the Blood-Nerve-Barrier in Diabetic Neuropathy. *Front Neurosci* **12**, 1038 (2018).
52. Sims, D.E. Diversity within pericytes. *Clin Exp Pharmacol Physiol* **27**, 842-846 (2000).
53. Jimenez-Andrade, J.M.*, et al.* Vascularization of the dorsal root ganglia and peripheral nerve of the mouse: implications for chemical-induced peripheral sensory neuropathies. *Molecular pain* **4**, 10 (2008).

54. Reinhold, A.K. & Rittner, H.L. Barrier function in the peripheral and central nervous system-a review. *Pflugers Arch* **469**, 123-134 (2017).
55. Kiernan, J.A. Vascular permeability in the peripheral autonomic and somatic nervous systems: controversial aspects and comparisons with the blood-brain barrier. *Microsc Res Tech* **35**, 122-136 (1996).
56. Hirakawa, H.*, et al.* Regional differences in blood-nerve barrier function and tight-junction protein expression within the rat dorsal root ganglion. *Neuroreport* **15**, 405-408 (2004).
57. Stierli, S.*, et al.* The regulation of the homeostasis and regeneration of peripheral nerve is distinct from the CNS and independent of a stem cell population. *Development* **145** (2018).
58. Zeng, G.*, et al.* Orientation of endothelial cell division is regulated by VEGF signaling during blood vessel formation. *Blood* **109**, 1345-1352 (2007).
59. Napoli, I.*, et al.* A central role for the ERK-signaling pathway in controlling Schwann cell plasticity and peripheral nerve regeneration in vivo. *Neuron* **73**, 729-742 (2012).
60. Mellick, R.S. & Cavanagh, J.B. Changes in blood vessel permeability during degeneration and regeneration in peripheral nerves. *Brain : a journal of neurology* **91**, 141-160 (1968).
61. Jessen, K.R. & Arthur-Farraj, P. Repair Schwann cell update: Adaptive reprogramming, EMT, and stemness in regenerating nerves. *Glia* **67**, 421-437 (2019).
62. Chan, J.R.*, et al.* NGF controls axonal receptivity to myelination by Schwann cells or oligodendrocytes. *Neuron* **43**, 183-191 (2004).
63. Lim, T.K.*, et al.* Blood-nerve barrier dysfunction contributes to the generation of neuropathic pain and allows targeting of injured nerves for pain relief. *Pain* **155**, 954-967 (2014).
64. Hashimoto, M.*, et al.* Neuroprotective effect of sonic hedgehog up-regulated in Schwann cells following sciatic nerve injury. *J Neurochem* **107**, 918-927 (2008).
65. Martinez, J.A.*, et al.* Intrinsic facilitation of adult peripheral nerve regeneration by the Sonic hedgehog morphogen. *Experimental neurology* **271**, 493-505 (2015).
66. Yu, F.X. & Guan, K.L. The Hippo pathway: regulators and regulations. *Genes Dev* **27**, 355-371 (2013).
67. Zhao, B., Tumaneng, K. & Guan, K.L. The Hippo pathway in organ size control, tissue regeneration and stem cell self-renewal. *Nat Cell Biol* **13**, 877-883 (2011).
68. Yu, X.*, et al.* Dorsal root ganglion macrophages contribute to both the initiation and persistence of neuropathic pain. *Nat Commun* **11**, 264 (2020).
69. Ydens, E.*, et al.* Profiling peripheral nerve macrophages reveals two macrophage subsets with distinct localization, transcriptome and response to injury. *Nature neuroscience* **23**, 676-689 (2020).
70. Wang, P.L.*, et al.* Peripheral nerve resident macrophages share tissue-specific programming and features of activated microglia. *Nat Commun* **11**, 2552 (2020).
71. Komori, T., Morikawa, Y., Inada, T., Hisaoka, T. & Senba, E. Site-specific subtypes of macrophages recruited after peripheral nerve injury. *Neuroreport* **22**, 911-917 (2011).
72. Lindborg, J.A.*, et al.* Molecular and cellular identification of the immune response in peripheral ganglia following nerve injury. *J Neuroinflammation* **15**, 192 (2018).
73. Hanani, M. Satellite glial cells in sensory ganglia: from form to function. *Brain Res Brain Res Rev* **48**, 457-476 (2005).

74. Doyle, J.P.*, et al.* Application of a translational profiling approach for the comparative analysis of CNS cell types. *Cell* **135**, 749-762 (2008).
75. Rabah, Y., Rubino, B., Moukarzel, E. & Agulhon, C. Characterization of transgenic mouse lines for selectively targeting satellite glial cells and macrophages in dorsal root ganglia. *PloS one* **15**, e0229475 (2020).
76. Zhang, Y.*, et al.* An RNA-sequencing transcriptome and splicing database of glia, neurons, and vascular cells of the cerebral cortex. *The Journal of neuroscience : the official journal of the Society for Neuroscience* **34**, 11929-11947 (2014).
77. Wolbert, J.*, et al.* Redefining the heterogeneity of peripheral nerve cells in health and autoimmunity. *Proceedings of the National Academy of Sciences of the United States of America* (2020).
78. Watanabe, E., Hiyama, T.Y., Kodama, R. & Noda, M. NaX sodium channel is expressed in non-myelinating Schwann cells and alveolar type II cells in mice. *Neuroscience letters* **330**, 109-113 (2002).
79. Christie, K.*, et al.* Intraganglionic interactions between satellite cells and adult sensory neurons. *Mol Cell Neurosci* **67**, 1-12 (2015).
80. Xie, W., Strong, J.A. & Zhang, J.M. Early blockade of injured primary sensory afferents reduces glial cell activation in two rat neuropathic pain models. *Neuroscience* **160**, 847-857 (2009).
81. Zhang, P., Sun, Y. & Ma, L. ZEB1: at the crossroads of epithelial-mesenchymal transition, metastasis and therapy resistance. *Cell Cycle* **14**, 481-487 (2015).
82. Singh, S.K., Kagalwala, M.N., Parker-Thornburg, J., Adams, H. & Majumder, S. REST maintains self-renewal and pluripotency of embryonic stem cells. *Nature* **453**, 223-227 (2008).
83. Shin, J.E., Geisler, S. & DiAntonio, A. Dynamic regulation of SCG10 in regenerating axons after injury. *Experimental neurology* **252**, 1-11 (2014).
84. Ramer, M.S. & Bisby, M.A. Differences in sympathetic innervation of mouse DRG following proximal or distal nerve lesions. *Experimental neurology* **152**, 197-207 (1998).
85. Ramer, M.S., Murphy, P.G., Richardson, P.M. & Bisby, M.A. Spinal nerve lesion-induced mechanoallodynia and adrenergic sprouting in sensory ganglia are attenuated in interleukin-6 knockout mice. *Pain* **78**, 115-121 (1998).
86. Gomez-Sanchez, J.A.*, et al.* After Nerve Injury, Lineage Tracing Shows That Myelin and Remak Schwann Cells Elongate Extensively and Branch to Form Repair Schwann Cells, Which Shorten Radically on Remyelination. *The Journal of neuroscience : the official journal of the Society for Neuroscience* **37**, 9086-9099 (2017).
87. Clements, M.P.*, et al.* The Wound Microenvironment Reprograms Schwann Cells to Invasive Mesenchymal-like Cells to Drive Peripheral Nerve Regeneration. *Neuron* **96**, 98-114 e117 (2017).
88. Arthur-Farraj, P.J.*, et al.* Changes in the Coding and Non-coding Transcriptome and DNA Methylome that Define the Schwann Cell Repair Phenotype after Nerve Injury. *Cell reports* **20**, 2719-2734 (2017).
89. Serinagaoglu, Y., Pare, J., Giovannini, M. & Cao, X. Nf2-Yap signaling controls the expansion of DRG progenitors and glia during DRG development. *Developmental biology* **398**, 97-109 (2015).

90. Ramer, M.S., Kawaja, M.D., Henderson, J.T., Roder, J.C. & Bisby, M.A. Glial overexpression of NGF enhances neuropathic pain and adrenergic sprouting into DRG following chronic sciatic constriction in mice. *Neuroscience letters* **251**, 53-56 (1998).
91. Cafferty, W.B.*, et al.* Conditioning injury-induced spinal axon regeneration fails in interleukin-6 knock-out mice. *The Journal of neuroscience : the official journal of the Society for Neuroscience* **24**, 4432-4443 (2004).
92. Cao, Z.*, et al.* The cytokine interleukin-6 is sufficient but not necessary to mimic the peripheral conditioning lesion effect on axonal growth. *The Journal of neuroscience : the official journal of the Society for Neuroscience* **26**, 5565-5573 (2006).
93. Hu, P. & McLachlan, E.M. Macrophage and lymphocyte invasion of dorsal root ganglia after peripheral nerve lesions in the rat. *Neuroscience* **112**, 23-38 (2002).
94. Hanani, M. & Spray, D.C. Emerging importance of satellite glia in nervous system function and dysfunction. *Nat Rev Neurosci* **21**, 485-498 (2020).
95. Gerstner, J.R.*, et al.* Brain fatty acid binding protein (Fabp7) is diurnally regulated in astrocytes and hippocampal granule cell precursors in adult rodent brain. *PloS one* **3**, e1631 (2008).
96. Prada, I.*, et al.* REST/NRSF governs the expression of dense-core vesicle gliosecretion in astrocytes. *The Journal of cell biology* **193**, 537-549 (2011).
97. Moreno, S. & Ceru, M.P. In search for novel strategies towards neuroprotection and neuroregeneration: is PPARalpha a promising therapeutic target? *Neural Regen Res* **10**, 1409-1412 (2015).
98. Bogdanov, P., Hernandez, C., Corraliza, L., Carvalho, A.R. & Simo, R. Effect of fenofibrate on retinal neurodegeneration in an experimental model of type 2 diabetes. *Acta Diabetol* **52**, 113-122 (2015).
99. Chen, X.R.*, et al.* Neurological recovery-promoting, anti-inflammatory, and anti-oxidative effects afforded by fenofibrate, a PPAR alpha agonist, in traumatic brain injury. *J Neurotrauma* **24**, 1119-1131 (2007).
100. Almad, A., Lash, A.T., Wei, P., Lovett-Racke, A.E. & McTigue, D.M. The PPAR alpha agonist gemfibrozil is an ineffective treatment for spinal cord injured mice. *Experimental neurology* **232**, 309-317 (2011).
101. Staden, R. Methods for calculating the probabilities of finding patterns in sequences. *Comput Appl Biosci* **5**, 89-96 (1989).
102. Yu, G., Wang, L.G., Han, Y. & He, Q.Y. clusterProfiler: an R package for comparing biological themes among gene clusters. *OMICS* **16**, 284-287 (2012).
103. The Gene Ontology, C. The Gene Ontology Resource: 20 years and still GOing strong. *Nucleic acids research* **47**, D330-D338 (2019).
104. Ashburner, M.*, et al.* Gene ontology: tool for the unification of biology. The Gene Ontology Consortium. *Nat Genet* **25**, 25-29 (2000).

Figure1

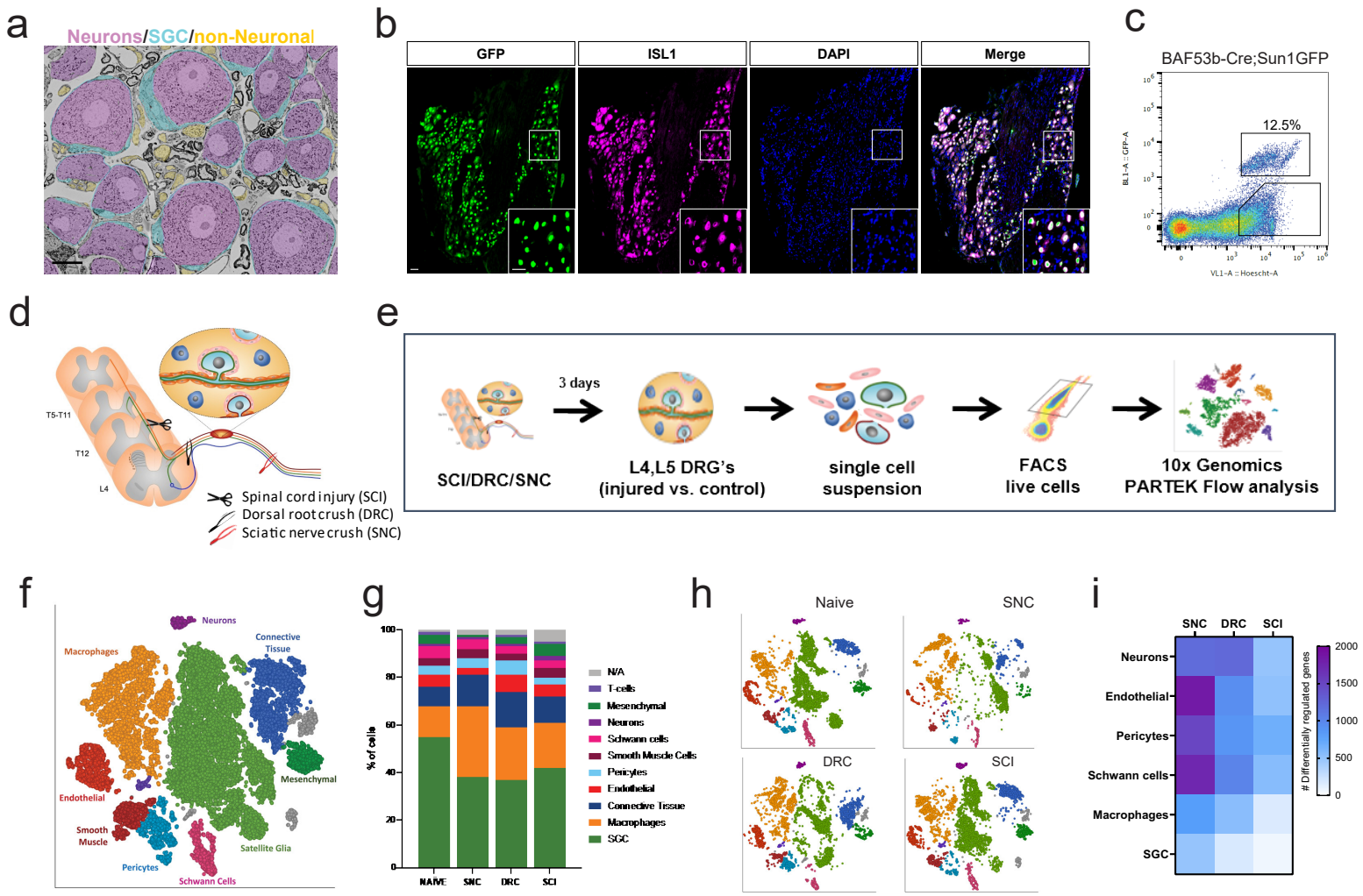
a
Neurons/SGC/non-Neuronal
b
GFP
ISL1
DAPI
Merge
c
BAF53b-Cre;Sun1GFP
12.5%
d
T5-T11
T12
L4
Spinal cord injury (SCI)
Dorsal root crush (DRC)
Sciatic nerve crush (SNC)
e
3 days
SCI/DRC/SNC
L4,L5 DRG's
(injured vs. control)
single cell
suspension
FACS
live cells
10x Genomics
PARTEK Flow analysis
f
Neurons
Connective Tissue
Macrophages
Mesenchymal
Endothelial
Smooth Muscle
Satellite Glia
Pericytes
Schwann Cells
g
% of cells
NAIVE
SNC
DRC
SCI
N/A
T-cells
Mesenchymal
Neurons
Schwann cells
Smooth Muscle Cells
Pericytes
Endothelial
Connective Tissue
Macrophages
SGC
h
Naive
SNC
DRC
SCI
i
SNC
DRC
SCI
Neurons
Endothelial
Pericytes
Schwann cells
Macrophages
SGC
Differentially regulated genes
2000
1500
1000
500
0

Figure2

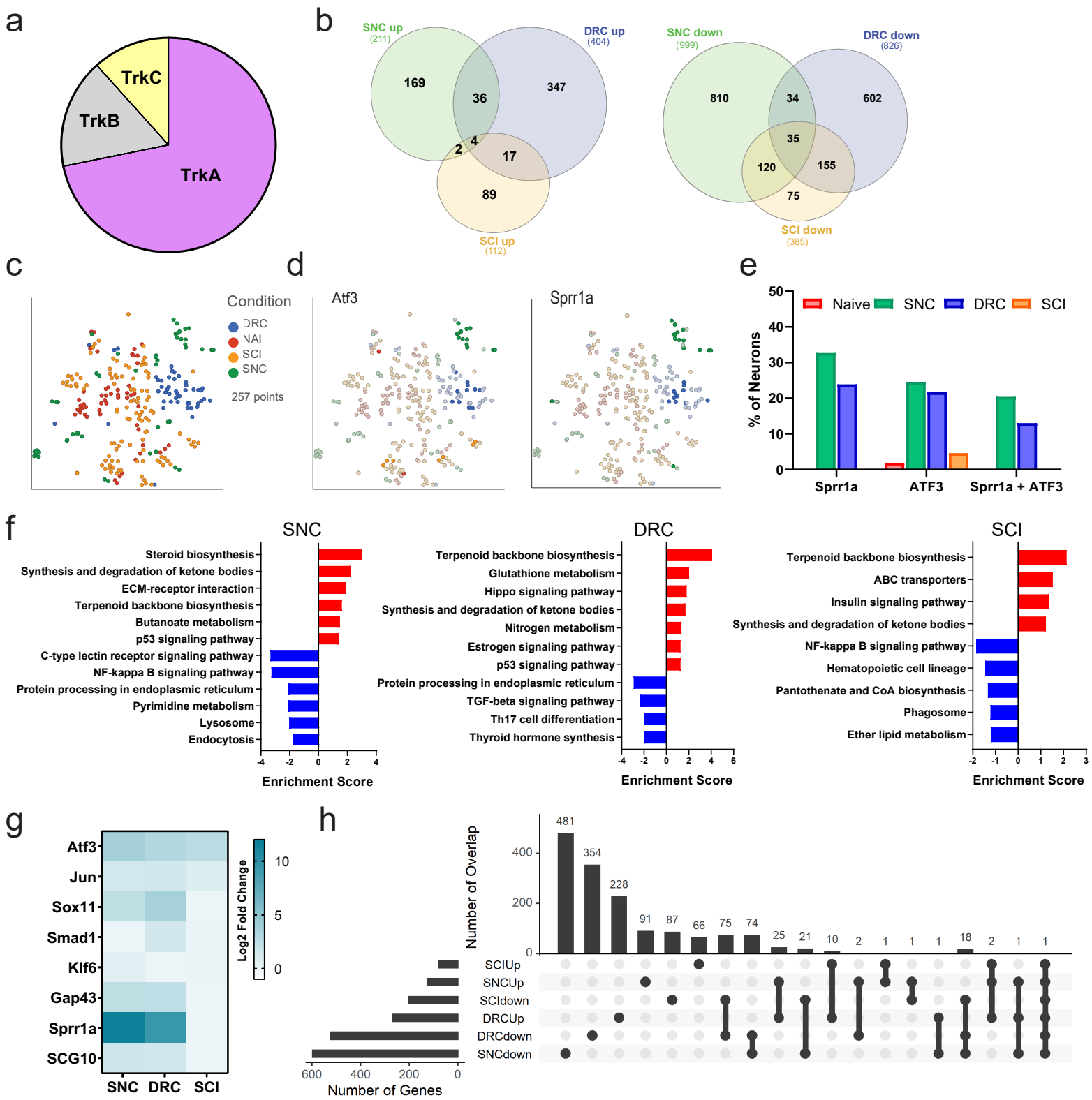
a
TrkC
TrkB
TrkA
b
SNC up
(211)
DRC up
(404)
169
36
347
2
4
17
89
SCI up
(112)
SNC down
(999)
DRC down
(826)
810
34
602
35
120
155
75
SCI down
(385)
c
Condition
DRC
NAI
SCI
SNC
257 points
d
Atf3
Sprr1a
e
Naive
SNC
DRC
SCI
% of Neurons
Sprr1a
ATF3
Sprr1a + ATF3
f
SNC
Steroid biosynthesis
Synthesis and degradation of ketone bodies
ECM-receptor interaction
Terpenoid backbone biosynthesis
Butanoate metabolism
p53 signaling pathway
C-type lectin receptor signaling pathway
NF-kappa B signaling pathway
Protein processing in endoplasmic reticulum
Pyrimidine metabolism
Lysosome
Endocytosis
Enrichment Score
DRC
Terpenoid backbone biosynthesis
Glutathione metabolism
Hippo signaling pathway
Synthesis and degradation of ketone bodies
Nitrogen metabolism
Estrogen signaling pathway
p53 signaling pathway
Protein processing in endoplasmic reticulum
TGF-beta signaling pathway
Th17 cell differentiation
Thyroid hormone synthesis
Enrichment Score
SCI
Terpenoid backbone biosynthesis
ABC transporters
Insulin signaling pathway
Synthesis and degradation of ketone bodies
NF-kappa B signaling pathway
Hematopoietic cell lineage
Pantothenate and CoA biosynthesis
Phagosome
Ether lipid metabolism
Enrichment Score
g
Atf3
Jun
Sox11
Smad1
Klf6
Gap43
Sprr1a
SCG10
SNC
DRC
SCI
Log2 Fold Change
h
Number of Overlap
481
354
228
91
87
66
75
74
25
21
10
2
1
1
1
18
2
1
1
SCIUp
SNCUp
SCIdown
DRCUp
DRCdown
SNCdown
Number of Genes

Figure3

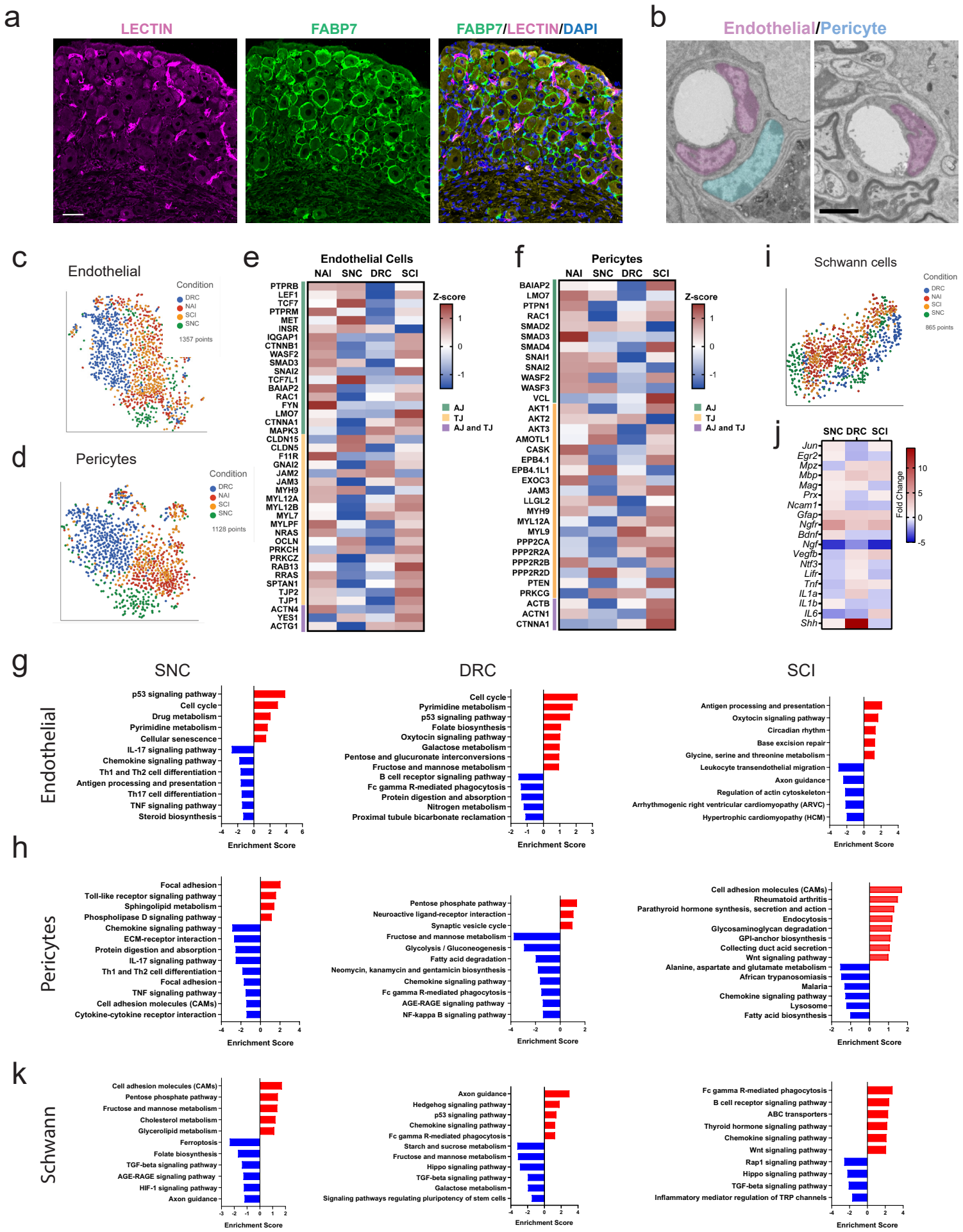
a
LECTIN
FABP7
FABP7/LECTIN/DAPI
b
Endothelial/Pericyte
c
Endothelial
Condition
DRC
NAI
SCI
SNC
1357 points
d
Pericytes
Condition
DRC
NAI
SCI
SNC
1128 points
e
Endothelial Cells
NAI SNC DRC SCI
PTPRB
LEF1
TCF7
PTPRM
MET
INSR
IQGAP1
CTNNB1
WASF2
SMAD3
SNAI2
TCF7L1
BAIAP2
RAC1
FYN
LMO7
CTNNA1
MAPK3
CLDN15
CLDN5
F11R
GNAI2
JAM2
JAM3
MYH9
MYL12A
MYL12B
MYL7
MYLPF
NRAS
OCLN
PRKCH
PRKCZ
RAB13
RRAS
SPTAN1
TJP2
TJP1
ACTN4
YES1
ACTG1
Z-score
1
0
-1
AJ
TJ
AJ and TJ
f
Pericytes
NAI SNC DRC SCI
BAIAP2
LMO7
PTPN1
RAC1
SMAD2
SMAD3
SMAD4
SNAI1
SNAI2
WASF2
WASF3
VCL
AKT1
AKT2
AKT3
AMOTL1
CASK
EPB4.1
EPB4.1L1
EXOC3
JAM3
LLGL2
MYH9
MYL12A
MYL9
PPP2CA
PPP2R2A
PPP2R2B
PPP2R2D
PTEN
PRKCG
ACTB
ACTN1
CTNNA1
Z-score
1
0
-1
AJ
TJ
AJ and TJ
i
Schwann cells
Condition
DRC
NAI
SCI
SNC
865 points
j
SNC DRC SCI
Jun
Egr2
Mpz
Mbp
Mag
Prx
Ncam1
Gfap
Ngfr
Bdnf
Ngf
Vegfb
Ntf3
Lifr
Tnf
IL1a
IL1b
IL6
Shh
Fold Change
10
5
0
-5
g
SNC
DRC
SCI
Endothelial
p53 signaling pathway
Cell cycle
Drug metabolism
Pyrimidine metabolism
Cellular senescence
IL-17 signaling pathway
Chemokine signaling pathway
Th1 and Th2 cell differentiation
Antigen processing and presentation
Th17 cell differentiation
TNF signaling pathway
Steroid biosynthesis
Enrichment Score
Cell cycle
Pyrimidine metabolism
p53 signaling pathway
Folate biosynthesis
Oxytocin signaling pathway
Galactose metabolism
Pentose and glucuronate interconversions
Fructose and mannose metabolism
B cell receptor signaling pathway
Fc gamma R-mediated phagocytosis
Protein digestion and absorption
Nitrogen metabolism
Proximal tubule bicarbonate reclamation
Enrichment Score
Antigen processing and presentation
Oxytocin signaling pathway
Circadian rhythm
Base excision repair
Glycine, serine and threonine metabolism
Leukocyte transendothelial migration
Axon guidance
Regulation of actin cytoskeleton
Arrhythmogenic right ventricular cardiomyopathy (ARVC)
Hypertrophic cardiomyopathy (HCM)
Enrichment Score
h
Pericytes
Focal adhesion
Toll-like receptor signaling pathway
Sphingolipid metabolism
Phospholipase D signaling pathway
Chemokine signaling pathway
ECM-receptor interaction
Protein digestion and absorption
IL-17 signaling pathway
Th1 and Th2 cell differentiation
Focal adhesion
TNF signaling pathway
Cell adhesion molecules (CAMs)
Cytokine-cytokine receptor interaction
Enrichment Score
Pentose phosphate pathway
Neuroactive ligand-receptor interaction
Synaptic vesicle cycle
Fructose and mannose metabolism
Glycolysis / Gluconeogenesis
Fatty acid degradation
Neomycin, kanamycin and gentamicin biosynthesis
Chemokine signaling pathway
Fc gamma R-mediated phagocytosis
AGE-RAGE signaling pathway
NF-kappa B signaling pathway
Enrichment Score
Cell adhesion molecules (CAMs)
Rheumatoid arthritis
Parathyroid hormone synthesis, secretion and action
Endocytosis
Glycosaminoglycan degradation
GPI-anchor biosynthesis
Collecting duct acid secretion
Wnt signaling pathway
Alanine, aspartate and glutamate metabolism
African trypanosomiasis
Malaria
Chemokine signaling pathway
Lysosome
Fatty acid biosynthesis
Enrichment Score
k
Schwann
Cell adhesion molecules (CAMs)
Pentose phosphate pathway
Fructose and mannose metabolism
Cholesterol metabolism
Glycerolipid metabolism
Ferroptosis
Folate biosynthesis
TGF-beta signaling pathway
AGE-RAGE signaling pathway
HIF-1 signaling pathway
Axon guidance
Enrichment Score
Axon guidance
Hedgehog signaling pathway
p53 signaling pathway
Chemokine signaling pathway
Fc gamma R-mediated phagocytosis
Starch and sucrose metabolism
Fructose and mannose metabolism
Hippo signaling pathway
TGF-beta signaling pathway
Galactose metabolism
Signaling pathways regulating pluripotency of stem cells
Enrichment Score
Fc gamma R-mediated phagocytosis
B cell receptor signaling pathway
ABC transporters
Thyroid hormone signaling pathway
Chemokine signaling pathway
Wnt signaling pathway
Rap1 signaling pathway
Hippo signaling pathway
TGF-beta signaling pathway
Inflammatory mediator regulation of TRP channels
Enrichment Score

Figure 4

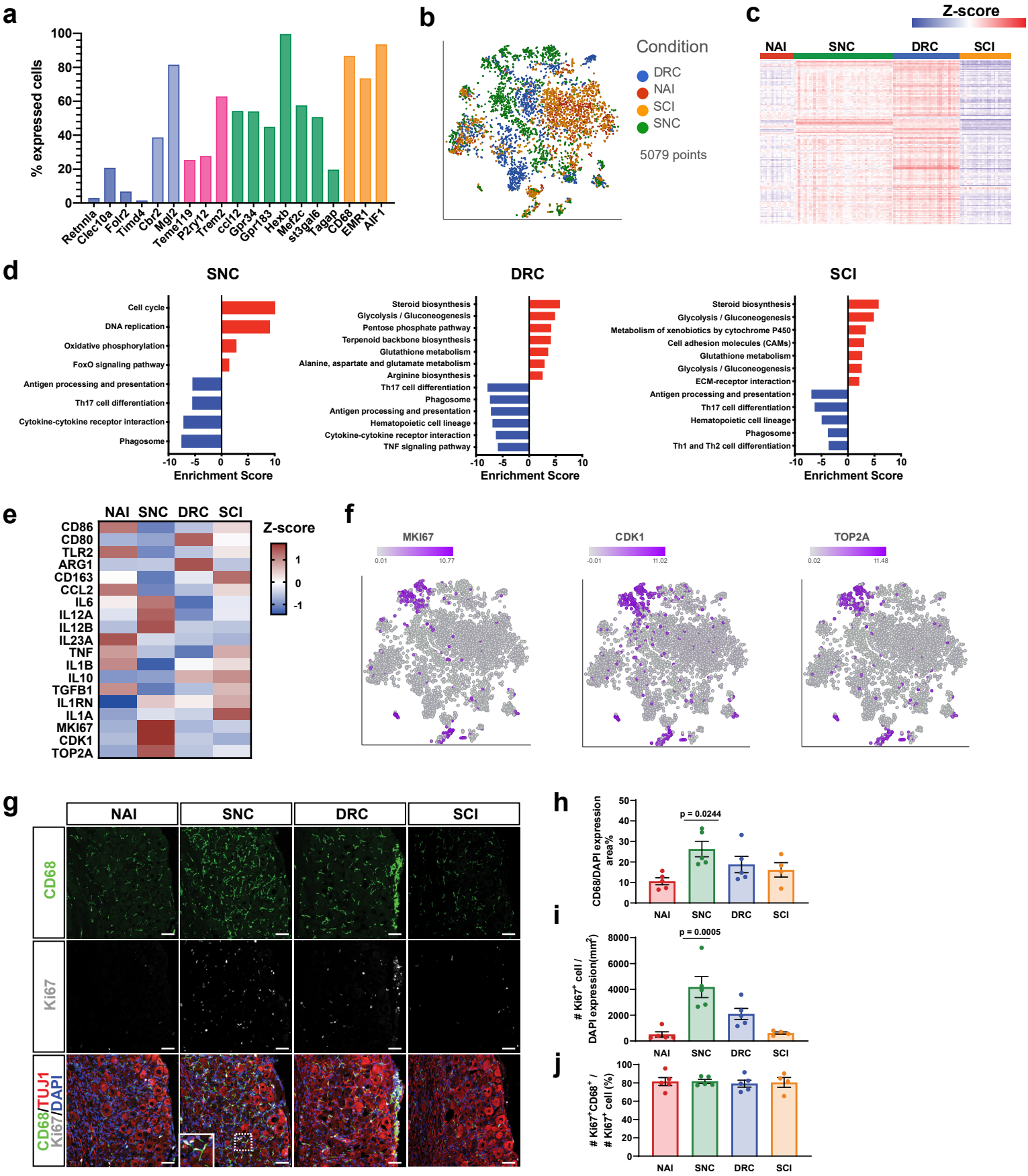
a
% expressed cells
Retnnla
Clec10a
Folr2
Timd4
Cbr2
Mgl2
Teme119
P2ry12
Trem2
ccl12
Gpr34
Gpr183
Hexb
Mef2c
st3gal6
Tagap
CD68
EMR1
AIF1
b
Condition
DRC
NAI
SCI
SNC
5079 points
c
Z-score
NAI
SNC
DRC
SCI
d
SNC
Cell cycle
DNA replication
Oxidative phosphorylation
FoxO signaling pathway
Antigen processing and presentation
Th17 cell differentiation
Cytokine-cytokine receptor interaction
Phagosome
Enrichment Score
DRC
Steroid biosynthesis
Glycolysis / Gluconeogenesis
Pentose phosphate pathway
Terpenoid backbone biosynthesis
Glutathione metabolism
Alanine, aspartate and glutamate metabolism
Arginine biosynthesis
Th17 cell differentiation
Phagosome
Antigen processing and presentation
Hematopoietic cell lineage
Cytokine-cytokine receptor interaction
TNF signaling pathway
Enrichment Score
SCI
Steroid biosynthesis
Glycolysis / Gluconeogenesis
Metabolism of xenobiotics by cytochrome P450
Cell adhesion molecules (CAMs)
Glutathione metabolism
Glycolysis / Gluconeogenesis
ECM-receptor interaction
Antigen processing and presentation
Th17 cell differentiation
Hematopoietic cell lineage
Phagosome
Th1 and Th2 cell differentiation
Enrichment Score
e
NAI SNC DRC SCI
CD86
CD80
TLR2
ARG1
CD163
CCL2
IL6
IL12A
IL12B
IL23A
TNF
IL1B
IL10
TGFB1
IL1RN
IL1A
MKI67
CDK1
TOP2A
Z-score
f
MKI67
CDK1
TOP2A
g
NAI
SNC
DRC
SCI
CD68
Ki67
CD68/TUJ1
Ki67/DAPI
h
CD68/DAPI expression area%
p = 0.0244
NAI
SNC
DRC
SCI
i
# Ki67+ cell / DAPI expression(mm2)
p = 0.0005
NAI
SNC
DRC
SCI
j
Ki67+CD68+ / # Ki67+ cell (%)
NAI
SNC
DRC
SCI

Figure5

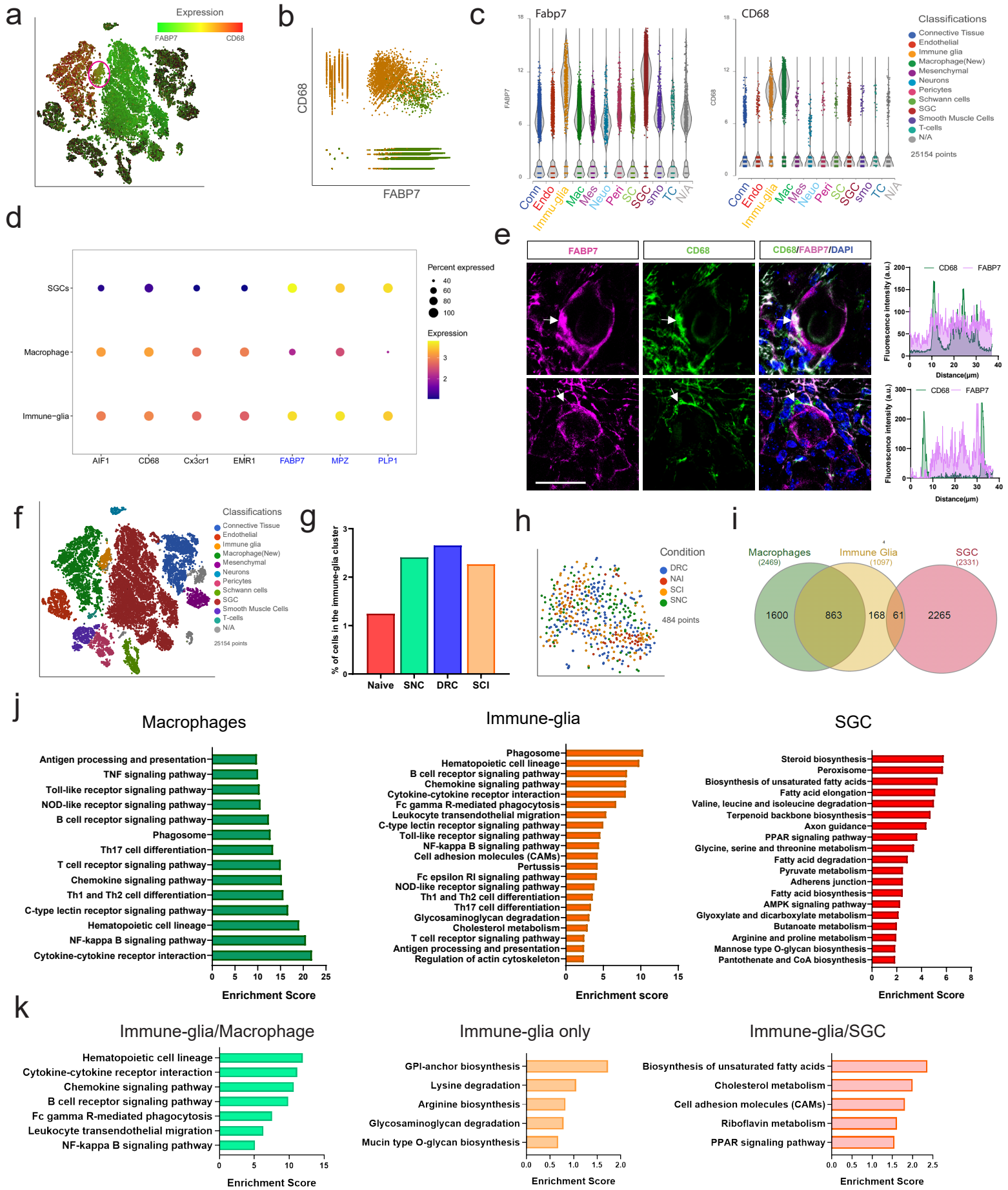
a
Expression
FABP7
CD68
b
CD68
FABP7
c
Fabp7
CD68
FABP7
Classifications
Connective Tissue
Endothelial
Immune glia
Macrophage(New)
Mesenchymal
Neurons
Pericytes
Schwann cells
SGC
Smooth Muscle Cells
T-cells
N/A
25154 points
Conn
Endo
Immu-glia
Mac
Mes
Neuro
Peri
SC
SGC
smo
TC
N/A
d
SGCs
Macrophage
Immune-glia
AIF1
CD68
Cx3cr1
EMR1
FABP7
MPZ
PLP1
Percent expressed
40
60
80
100
Expression
3
2
e
FABP7
CD68
CD68/FABP7/DAPI
Fluorescence intensity (a.u.)
Distance(μm)
f
Classifications
Connective Tissue
Endothelial
Immune glia
Macrophage(New)
Mesenchymal
Neurons
Pericytes
Schwann cells
SGC
Smooth Muscle Cells
T-cells
N/A
25154 points
g
% of cells in the immune-glia cluster
Naive
SNC
DRC
SCI
h
Condition
DRC
NAI
SCI
SNC
484 points
i
Macrophages
(2469)
Immune Glia
(1097)
SGC
(2331)
1600
863
168
61
2265
j
Macrophages
Antigen processing and presentation
TNF signaling pathway
Toll-like receptor signaling pathway
NOD-like receptor signaling pathway
B cell receptor signaling pathway
Phagosome
Th17 cell differentiation
T cell receptor signaling pathway
Chemokine signaling pathway
Th1 and Th2 cell differentiation
C-type lectin receptor signaling pathway
Hematopoietic cell lineage
NF-kappa B signaling pathway
Cytokine-cytokine receptor interaction
Enrichment Score
Immune-glia
Phagosome
Hematopoietic cell lineage
B cell receptor signaling pathway
Chemokine signaling pathway
Cytokine-cytokine receptor interaction
Fc gamma R-mediated phagocytosis
Leukocyte transendothelial migration
C-type lectin receptor signaling pathway
Toll-like receptor signaling pathway
NF-kappa B signaling pathway
Cell adhesion molecules (CAMs)
Pertussis
Fc epsilon RI signaling pathway
NOD-like receptor signaling pathway
Th1 and Th2 cell differentiation
Th17 cell differentiation
Glycosaminoglycan degradation
Cholesterol metabolism
T cell receptor signaling pathway
Antigen processing and presentation
Regulation of actin cytoskeleton
Enrichment score
SGC
Steroid biosynthesis
Peroxisome
Biosynthesis of unsaturated fatty acids
Fatty acid elongation
Valine, leucine and isoleucine degradation
Terpenoid backbone biosynthesis
Axon guidance
PPAR signaling pathway
Glycine, serine and threonine metabolism
Fatty acid degradation
Pyruvate metabolism
Adherens junction
Fatty acid biosynthesis
AMPK signaling pathway
Glyoxylate and dicarboxylate metabolism
Butanoate metabolism
Arginine and proline metabolism
Mannose type O-glycan biosynthesis
Pantothenate and CoA biosynthesis
Enrichment Score
k
Immune-glia/Macrophage
Hematopoietic cell lineage
Cytokine-cytokine receptor interaction
Chemokine signaling pathway
B cell receptor signaling pathway
Fc gamma R-mediated phagocytosis
Leukocyte transendothelial migration
NF-kappa B signaling pathway
Enrichment Score
Immune-glia only
GPI-anchor biosynthesis
Lysine degradation
Arginine biosynthesis
Glycosaminoglycan degradation
Mucin type O-glycan biosynthesis
Enrichment Score
Immune-glia/SGC
Biosynthesis of unsaturated fatty acids
Cholesterol metabolism
Cell adhesion molecules (CAMs)
Riboflavin metabolism
PPAR signaling pathway
Enrichment Score

Figure6

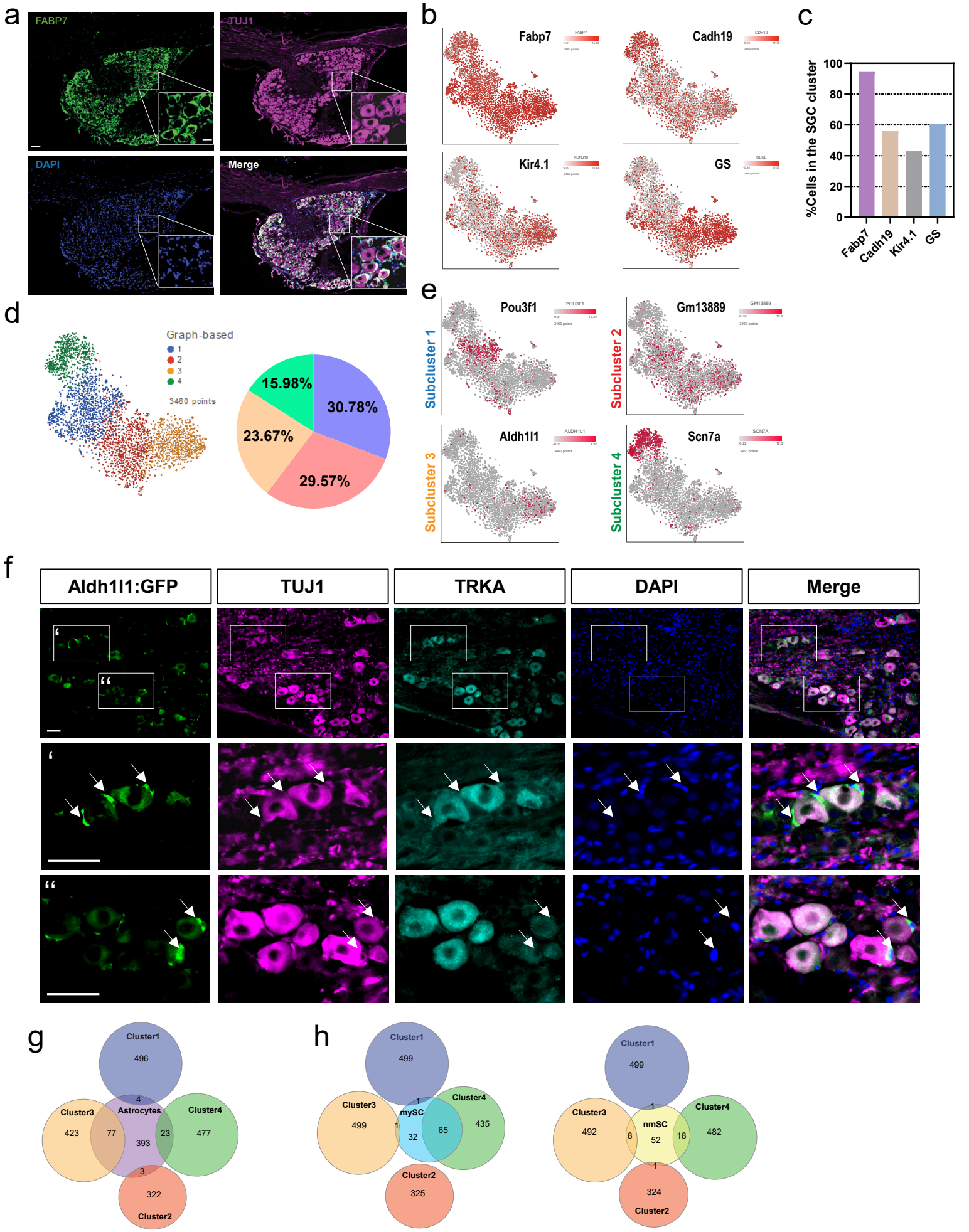
a
FABP7
TUJ1
DAPI
Merge
b
Fabp7
Cadh19
Kir4.1
GS
c
%Cells in the SGC cluster
100
80
60
40
20
0
Fabp7
Cadh19
Kir4.1
GS
d
Graph-based
1
2
3
4
3460 points
15.98%
30.78%
23.67%
29.57%
e
Subcluster 1
Pou3f1
Subcluster 2
Gm13889
Subcluster 3
Aldh1l1
Subcluster 4
Scn7a
f
Aldh1l1:GFP
TUJ1
TRKA
DAPI
Merge
g
Cluster1
496
4
Astrocytes
Cluster3
423
77
393
23
Cluster4
477
3
322
Cluster2
h
Cluster1
499
1
Cluster3
499
1
mySC
32
65
Cluster4
435
Cluster2
325
Cluster1
499
1
Cluster3
492
8
nmSC
52
18
Cluster4
482
1
324
Cluster2

Figure7

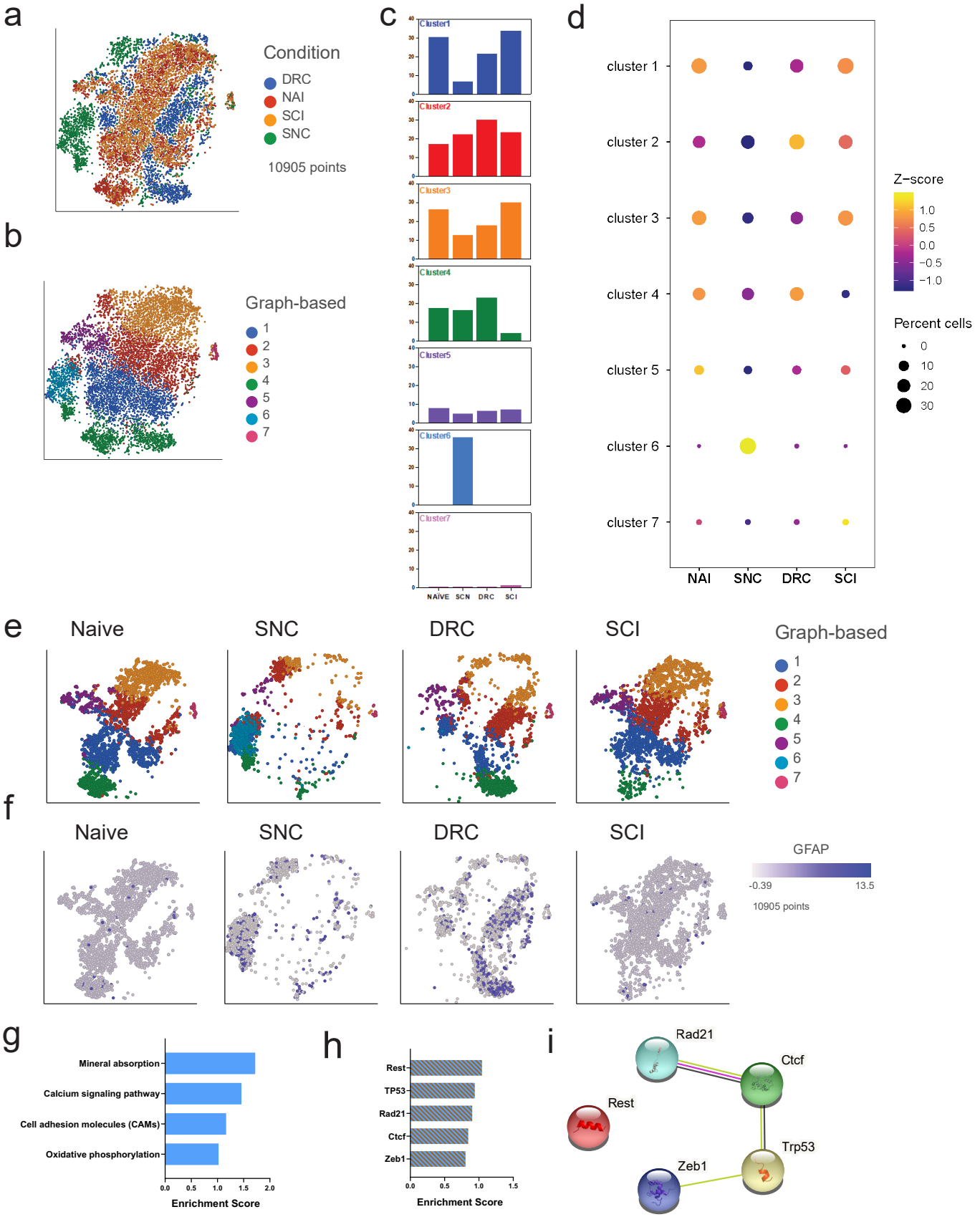
a
Condition
DRC
NAI
SCI
SNC
10905 points
b
Graph-based
1
2
3
4
5
6
7
c
Cluster1
Cluster2
Cluster3
Cluster4
Cluster5
Cluster6
Cluster7
NAIVE
SCN
DRC
SCI
d
cluster 1
cluster 2
cluster 3
cluster 4
cluster 5
cluster 6
cluster 7
NAI
SNC
DRC
SCI
Z−score
1.0
0.5
0.0
−0.5
−1.0
Percent cells
0
10
20
30
e
Naive
SNC
DRC
SCI
Graph-based
1
2
3
4
5
6
7
f
Naive
SNC
DRC
SCI
GFAP
-0.39
13.5
10905 points
g
Mineral absorption
Calcium signaling pathway
Cell adhesion molecules (CAMs)
Oxidative phosphorylation
0.0
0.5
1.0
1.5
2.0
Enrichment Score
h
Rest
TP53
Rad21
Ctcf
Zeb1
0.0
0.5
1.0
1.5
Enrichment Score
i
Rad21
Ctcf
Rest
Trp53
Zeb1

Figure8

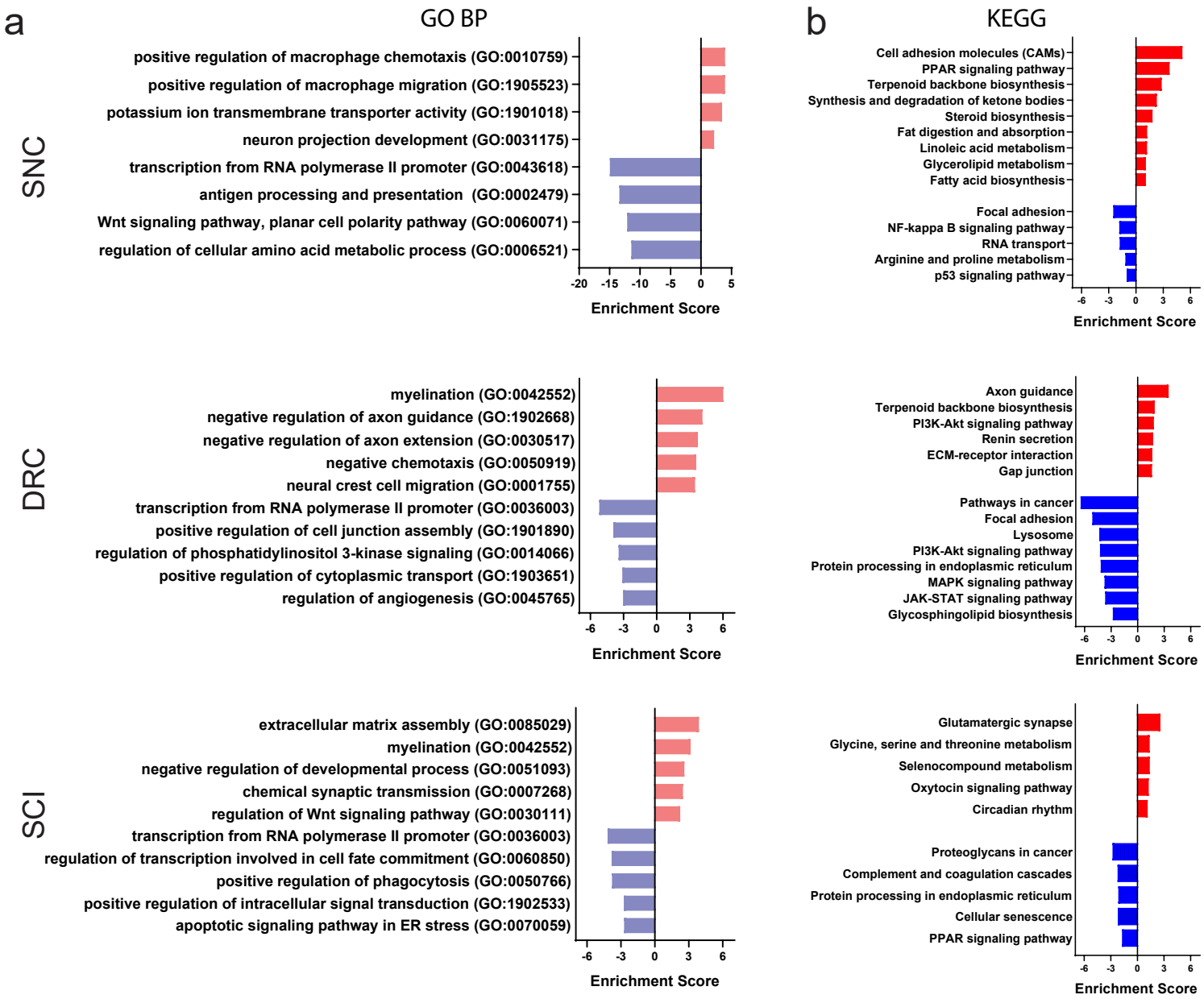
a
GO BP
SNC
positive regulation of macrophage chemotaxis (GO:0010759)
positive regulation of macrophage migration (GO:1905523)
potassium ion transmembrane transporter activity (GO:1901018)
neuron projection development (GO:0031175)
transcription from RNA polymerase II promoter (GO:0043618)
antigen processing and presentation (GO:0002479)
Wnt signaling pathway, planar cell polarity pathway (GO:0060071)
regulation of cellular amino acid metabolic process (GO:0006521)
-20 -15 -10 -5 0 5
Enrichment Score
b
KEGG
Cell adhesion molecules (CAMs)
PPAR signaling pathway
Terpenoid backbone biosynthesis
Synthesis and degradation of ketone bodies
Steroid biosynthesis
Fat digestion and absorption
Linoleic acid metabolism
Glycerolipid metabolism
Fatty acid biosynthesis
Focal adhesion
NF-kappa B signaling pathway
RNA transport
Arginine and proline metabolism
p53 signaling pathway
-6 -3 0 3 6
Enrichment Score
DRC
myelination (GO:0042552)
negative regulation of axon guidance (GO:1902668)
negative regulation of axon extension (GO:0030517)
negative chemotaxis (GO:0050919)
neural crest cell migration (GO:0001755)
transcription from RNA polymerase II promoter (GO:0036003)
positive regulation of cell junction assembly (GO:1901890)
regulation of phosphatidylinositol 3-kinase signaling (GO:0014066)
positive regulation of cytoplasmic transport (GO:1903651)
regulation of angiogenesis (GO:0045765)
-6 -3 0 3 6
Enrichment Score
Axon guidance
Terpenoid backbone biosynthesis
PI3K-Akt signaling pathway
Renin secretion
ECM-receptor interaction
Gap junction
Pathways in cancer
Focal adhesion
Lysosome
PI3K-Akt signaling pathway
Protein processing in endoplasmic reticulum
MAPK signaling pathway
JAK-STAT signaling pathway
Glycosphingolipid biosynthesis
-6 -3 0 3 6
Enrichment Score
SCI
extracellular matrix assembly (GO:0085029)
myelination (GO:0042552)
negative regulation of developmental process (GO:0051093)
chemical synaptic transmission (GO:0007268)
regulation of Wnt signaling pathway (GO:0030111)
transcription from RNA polymerase II promoter (GO:0036003)
regulation of transcription involved in cell fate commitment (GO:0060850)
positive regulation of phagocytosis (GO:0050766)
positive regulation of intracellular signal transduction (GO:1902533)
apoptotic signaling pathway in ER stress (GO:0070059)
-6 -3 0 3 6
Enrichment Score
Glutamatergic synapse
Glycine, serine and threonine metabolism
Selenocompound metabolism
Oxytocin signaling pathway
Circadian rhythm
Proteoglycans in cancer
Complement and coagulation cascades
Protein processing in endoplasmic reticulum
Cellular senescence
PPAR signaling pathway
-6 -3 0 3 6
Enrichment Score
c
Control Diet
Fenofibrate Diet
d
p=0.0294
10 Longests Axons (μm)
0 200 400 600 800 1000 1200 1400
Control Diet
Fenofibrate Diet
e
Control Diet
Fenofibrate Diet
ns
p=0.0003
p<0.0001
p<0.0001
p=0.0034
Regeneration Index(%)
0 20 40 60 80 100
100 200 300 400 800
Distance from injury site (μm)

Supplementary figure 1

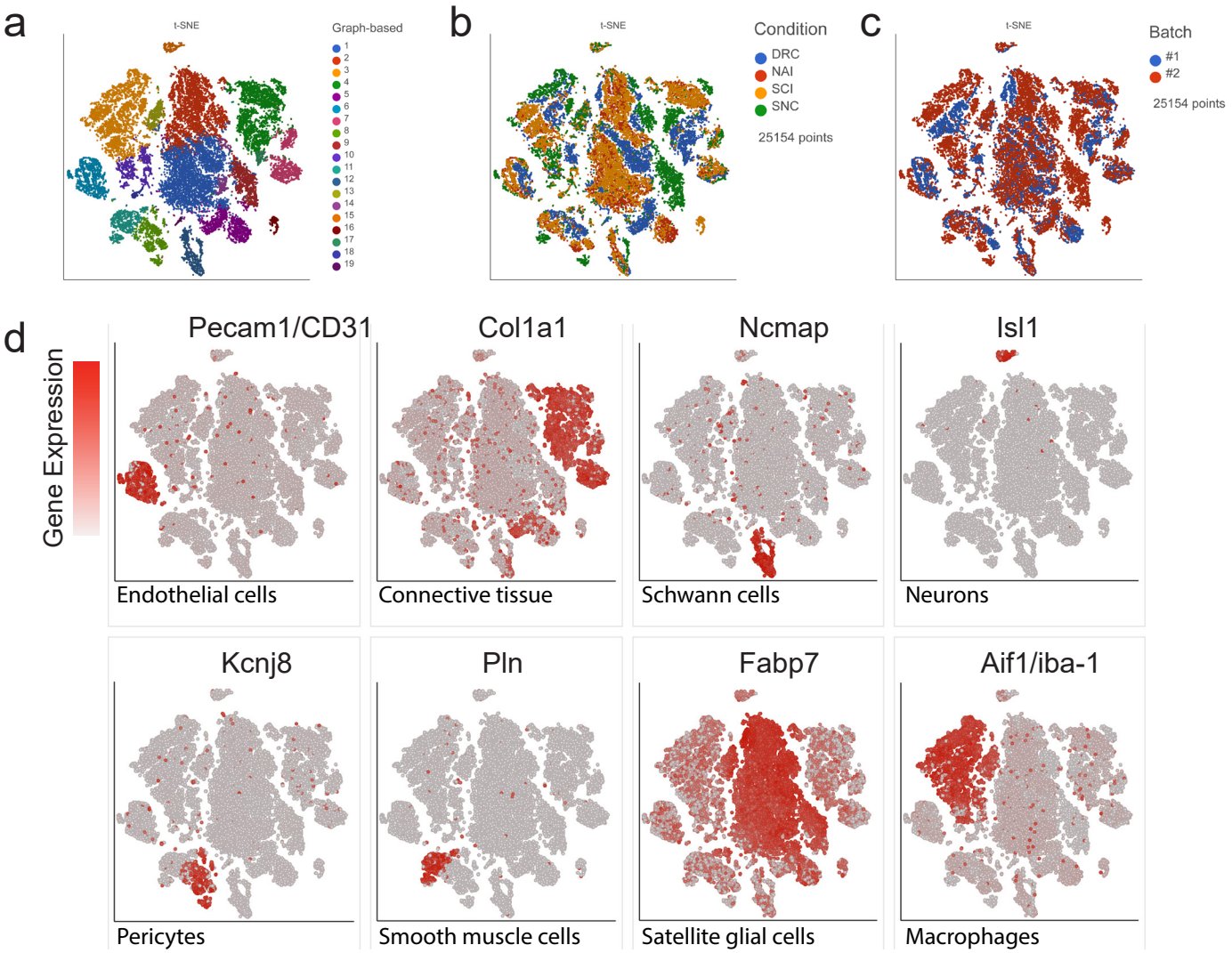

Supplementary Figure2

a

b

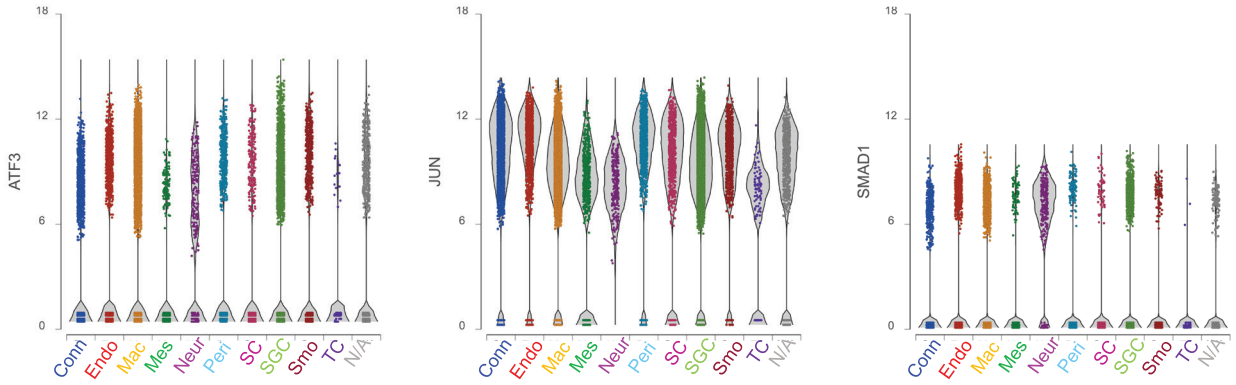

c

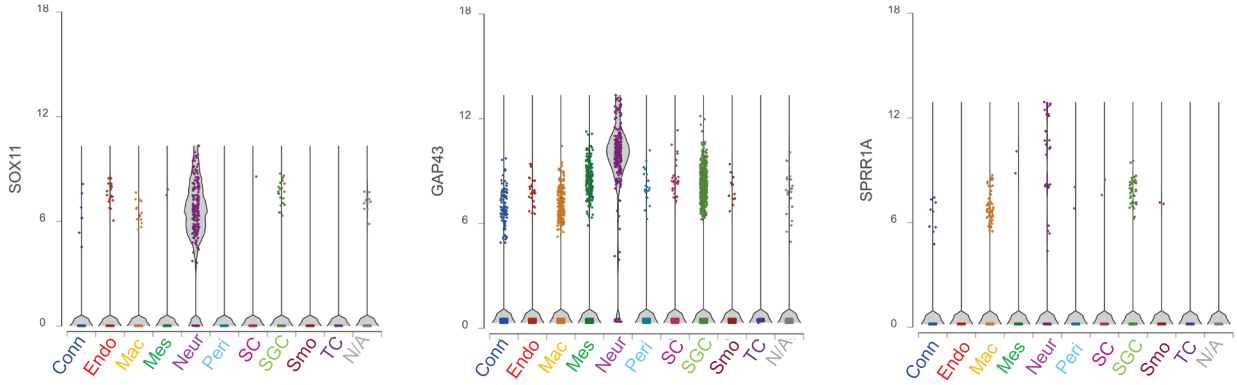
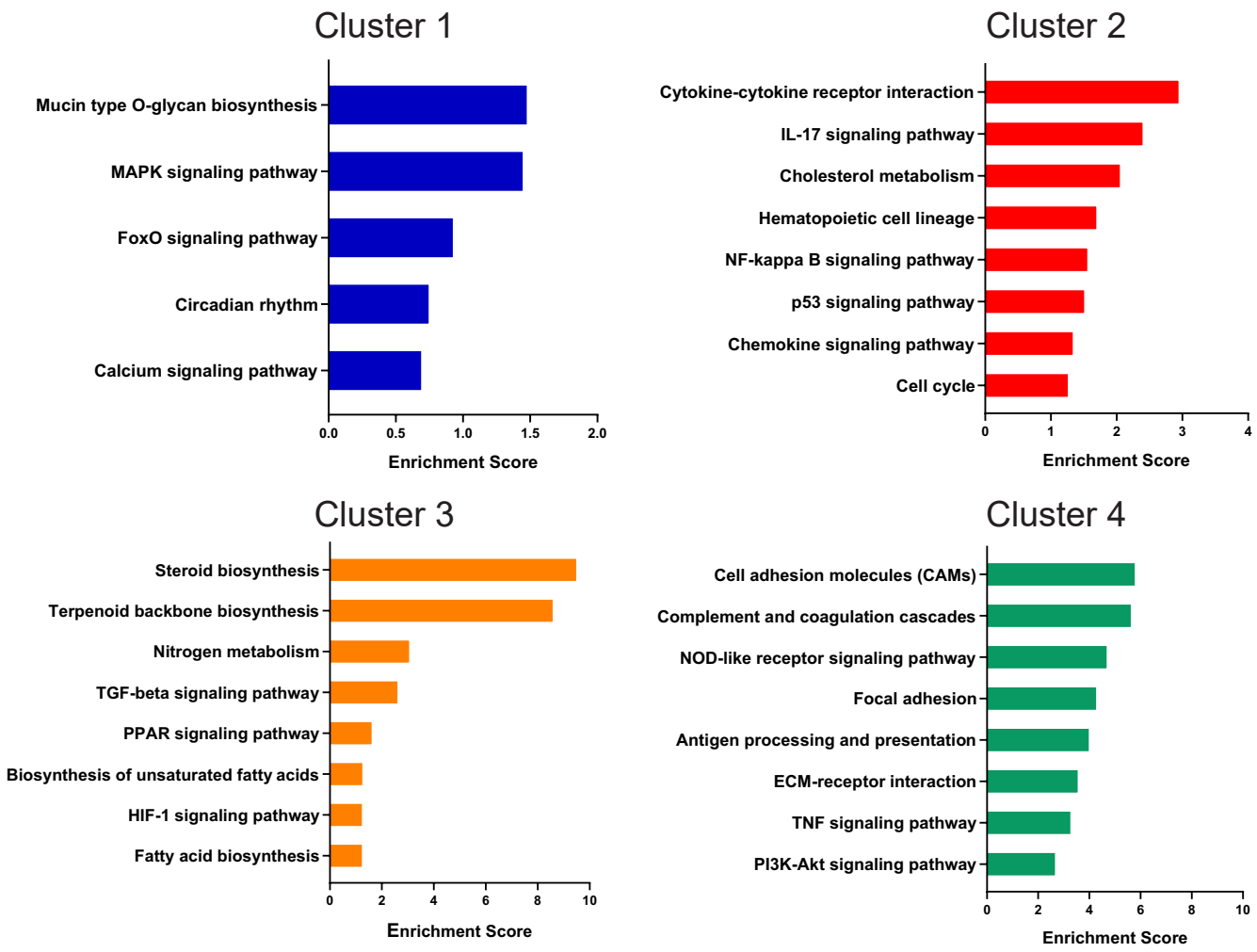
Supplementary figure 3